BrainPalmSeq: A curated RNA-seq database of palmitoylating and de-palmitoylating enzyme expression in the mouse brain

Authors: Wild, AR[1]; Hogg, PW[1]; Flibotte, S[2]; Nasseri, G[1]; Hollman, R[1]; Haas, K[1] and Bamji, SX[1]

Affiliations:

1 Department of Cellular and Physiological Sciences, Life Sciences Institute and Djavad Mowafaghian Centre for Brain Health, University of British Columbia

2 Life Sciences Institute Bioinformatics Facility, University of British Columbia

Correspondence:
Shernaz Bamji, Ph.D.
Department of Cellular and Physiological Sciences
Life Sciences Institute,
Djavad Mowafaghian Centre for Brain Health
University of British Columbia
2350 Health Sciences Mall
Vancouver, B.C., V6T 1Z3
Off: 604-822-4746

Abstract

Protein *S*-palmitoylation is a reversible post translational lipid modification that plays a critical role in neuronal development and plasticity, while dysregulated *S*-palmitoylation underlies a number of severe neurological disorders. Dynamic *S*-palmitoylation is regulated by a large family of ZDHHC palmitoylating enzymes, their accessory proteins, and a small number of known de-palmitoylating enzymes. Here, we curated and analyzed expression data for the proteins that mediate *S*-palmitoylation from publicly available RNAseq datasets, providing a comprehensive overview of their distribution in the mouse nervous system. We developed a web-tool that enables interactive visualization of the expression patterns for these proteins in the nervous system (http://brainpalmseq.med.ubc.ca/), and explored this resource to find region and cell-type specific expression patterns that give insight into the function of palmitoylating and de-palmitoylating enzymes in the brain and neurological disorders. We found coordinated expression of ZDHHC enzymes with their accessory proteins, de-palmitoylating enzymes and other brain-expressed genes that included an enrichment of *S*-palmitoylation substrates. Finally, we utilized ZDHHC expression patterns to predict and validate palmitoylating enzyme-substrate interactions.

Introduction

Protein *S*-palmitoylation is a post-translational lipid modification that mediates dynamic changes in protein stability, function, and membrane localization. *S*-palmitoylation is defined as the reversible formation of a cysteine residue thioester bond with the fatty acid palmitate, and is the most prevalent post translational lipid modification in the brain. Dynamic changes in *S*-palmitoylation are critical for neuronal development and synaptic plasticity (Fukata et al., 2013; Fukata and Fukata, 2010; Globa and Bamji, 2017; Matt et al., 2019), oligodendrocyte differentiation and myelination (Ma et al., 2021; Schneider et al., 2005), and astrocyte proliferation (Yuan et al., 2021). Furthermore, numerous neurological and psychiatric diseases have now been attributed to mutations in the genes encoding palmitoylating and de-palmitoylating enzymes, including schizophrenia, intellectual disability and CLN1 disease (Mukai et al., 2004; Nita et al., 2016; Raymond et al., 2007), underscoring the importance of properly regulated *S*-palmitoylation in normal brain function.

S-Palmitoylation is mediated by a family of ZDHHC enzymes that share a consensus 'asp-his-his-cys' catalytic domain. These enzymes are structurally heterogeneous multi-pass transmembrane proteins that localize to a variety of intracellular compartments, including the golgi, endoplasmic reticulum (ER), recycling endosomes and the plasma membrane (Globa and Bamji, 2017). The ZDHHC enzymes are known

61 to be associated with accessory proteins that regulate their stability, activity, and trafficking (Salaun et al.,
62 2020). Several de-palmitoylating enzymes have also been identified that act as the 'erasers' of *S*-
63 palmitoylation, and are divided into three classes: the acyl-protein thioesterases that shuttle between the
64 golgi and cytosol (APTs; Vartak et al., 2014), the predominantly lysosomal palmitoyl-protein thioesterases
65 (PPTs; Koster and Yoshii, 2019) and the more recently discovered α/β hydrolase domain-containing 17
66 proteins (ABHD17; Lin and Conibear, 2015). Unlike other post-translational modifications, palmitoylation
67 lacks a consensus substrate amino sequence, and the mechanisms that govern ZDHHC enzyme-substrate
68 interactions are controversial, with contrasting reports of substrate interactions being both promiscuous
69 and specific (Malgapo and Linder, 2021). Currently these interactions are thought to be governed by the
70 subcellular targeting of ZDHHCs enzymes and the presence of protein-protein interacting motifs within
71 the ZDHHC N- and C-termini, which are highly diverse among the ZDHHC enzymes (Rana et al., 2018).
72 Differential gene expression can also have a profound influence on protein interactions, and may play a
73 role in the coordination of *S*-palmitoylation in the brain. However, a detailed overview and analysis of the
74 precise cellular and regional expression patterns of the palmitoylating and de-palmitoylating enzymes has
75 not yet been described, and as such little is known about how this expression is coordinated in the nervous
76 system.

77 Recent advances in single-cell RNA sequencing (scRNAseq) techniques have enabled the
78 classification of neuronal and non-neuronal cell types in unprecedented detail, providing a better
79 understanding of cellular diversity and function in the nervous system, while also providing a means to
80 study the expression patterns of individual genes across an ever-expanding range of brain regions and
81 cellular classifications. Here, we capitalized on the recent surge in RNAseq publications characterizing
82 regional and cellular transcriptomics of the mouse nervous system. We curated and analyzed expression
83 data from a number of publicly available RNAseq mouse datasets to generate a detailed analysis of the
84 expression patterns of the genes associated with *S*-palmitoylation in the mouse brain. Furthermore, we
85 present an interactive web tool to allow user-driven interrogation of the expression patterns of
86 palmitoylating and de-palmitoylating enzymes from numerous collated studies across a variety of brain
87 regions and cell-types (http://brainpalmseq.med.ubc.ca/). We demonstrate the utility of this resource by
88 detailing the considerable cell type and regional heterogeneity in expression patterns of these enzyme
89 families and their accessory proteins, revealing numerous cell type enrichments and co-expression
90 patterns that allowed us to generate and test hypotheses about palmitoylating enzyme-substrate
91 interactions.

Results

BrainPalmSeq: an interactive database to search palmitoylating and depalmitoylating enzyme expression in the mouse brain

The recent development of scRNAseq has revolutionized our understanding of the complex transcriptional diversity of neuronal and non-neuronal cell types in the brain. We found however, there were several barriers to the easy access for much of this data, with no single resource available to evaluate multi-study expression data. Data can also be difficult to access when studies are not accompanied by an interactive online web viewer, while datasets that do have a web viewer employ diverse interfaces that are often complex, particularly for large scRNAseq datasets. Furthermore, the differing study specific analysis pipelines, as well as the variety of data presentation formats in web viewers including heatmaps, bar charts, tables or t-SNE plots can make datasets difficult for non-bioinformaticians to interpret and compare. In order to remove these barriers and provide easy access to expression data for the proteins that regulate *S*-palmitoylation in the brain, we created 'BrainPalmSeq', an easy-to-use web platform allowing user driven interrogation of compiled multi-study expression data at cellular resolution through simple interactive heatmaps that are populated according to user selected brain regions, cell-types or genes of interest (http://brainpalmseq.med.ubc.ca/).

To create BrainPalmSeq we first curated three large datasets from whole-brain scRNAseq studies to provide high resolution expression data covering hundreds of cell types at a variety of developmental ages, acquired through selection-free cell sampling (Rosenberg et al., 2018; Saunders et al., 2018; Zeisel et al., 2018). As scRNAseq has several caveats including low sensitivity and high frequency of dropout events leading to incomplete detection of expressed genes (Haque et al., 2017), we complement these datasets where possible with curation of several bulk and pooled-cell RNAseq studies that used population-level ensemble measurements from whole-brain and region-specific studies. We further include selected studies for the major glial cell types and data from the most comprehensive neuron specific study performed to date by the Allen Institute (Table S1). Together, the datasets curated in BrainPalmSeq cover all major regions of the mouse nervous system at a variety of sequencing resolutions.

Expression data were extracted from selected studies for the 24 mouse ZDHHC genes (*Zdhhc1*-*Zdhhc25*, while *Zdhhc10* is omitted), as well as the best characterized de-palmitoylating enzymes (*Ppt1*, *Lypla1*, *Lypla2*, *Abhd17a*, *Abhd17b* and *Abhd17c*) and ZDHHC accessory proteins (*Golga7*, *Golga7b* and *Selk*). Where possible, data were processed from the raw transcripts or unique molecular identifier (UMI) counts using the same normalization protocol to allow for more consistent evaluation of differences in

123 gene expression within datasets. We sampled from RNAseq datasets that used a diverse range of sample
124 collection, processing and analysis techniques, therefore the relative expression patterns of selected
125 genes can be directly visualized within datasets, and users can then validate their observations across
126 complimentary whole brain or region/cell-type specific datasets included in BrainPalmSeq. Dropdown
127 menus allow for selection of individual ZDHHC genes or brain regions within each dataset, while the hover
128 tool reveals metadata for each cell-type, including neurotransmitter designations and marker genes. We
129 provide download links to all expression data including cell-type metadata so that users can replot gene
130 expression profiles in their preferred format. To demonstrate the utility of this resource, we performed a
131 detailed exploration of selected datasets from BrainPalmSeq, revealing how expression patterns can give
132 insights into the function of the palmitoylating and de-palmitoylating enzymes in the mouse brain.

133 **ZDHHC expression in the nervous system shows regional and cell-type specific patterning**

134 We began by exploring BrainPalmSeq data curated from the 'MouseBrain' dataset, which provides
135 the broadest overview of expression patterns in the nervous system (Zeisel et al., 2018). This scRNAseq
136 study sampled multiple dissected regions from the adolescent (mean age ~P25) mouse central and
137 peripheral nervous systems (CNS and PNS), identifying 265 transcriptomically unique cell-types (referred
138 to herein as metacells) for which we plotted re-normalized ZDHHC expression values, according to the
139 hierarchical cell-type clustering established by the original study (Figure 1A). While ZDHHC expression was
140 detected in all regions of the nervous system, expression of the 24 ZDHHC genes was highly variable across
141 metacell types and clusters. We measured the mean ZDHHC expression within each cluster to gain insight
142 into which cell-types in the nervous system have the greatest overall expression of palmitoylating
143 enzymes. The heatmap rows and columns were ranked (sorted by averages descending) to determine
144 which cell-types had the highest expression of ZDHHCs, and which ZDHHCs were most abundantly
145 expressed across cell-types (Figure 1B). Mean ZDHHC expression was particularly high in neurons of the
146 PNS, along with cholinergic/monoaminergic and hindbrain neurons of the CNS. Of the non-neuronal
147 metacell clusters, oligodendrocytes had the highest ZDHHC expression, while other glial cell-types appear
148 at the lower end of the ranking (Figure 1B). *Zdhhc20* was the most abundantly expressed ZDHHC, with the
149 highest mean expression across all cell-type clusters, followed by *Zdhhc2*, *Zdhhc17*, *Zdhhc3* and *Zdhhc21*,
150 while expression of *Zdhhc11*, *Zdhhc19* and *Zdhhc25* was negligible. We next clustered neuronal metacells
151 of the PNS and CNS according to the neurotransmitter combinations, revealing the highest mean ZDHHC
152 expression was observed in neurons that utilized acetylcholine and nitric oxide as co-neurotransmitters,
153 with cholinergic neurons featuring near the top of the list in several neurotransmitter combinations
154 (Figure 1C). Monoaminergic neurons utilizing noradrenaline and serotonin also generally ranked high in

155 the list, consistent with the data in Figure 1B that ranked cholinergic and monoaminergic neurons as the
156 metacell cluster with the highest CNS ZDHHC expression overall, indicating a higher propensity for these
157 cell-types to utilize *S*-palmitoylation as a post-translational mechanism to modify cellular signaling. We
158 performed comparative analysis of ZDHHC expression on another large-scale scRNAseq study of the
159 mouse brain that sampled a variety of cortical and subcortical structures of the adult mouse (P60-P70)
160 (Saunders et al., 2018; 'DropViz'; Figure S1A). We found expression patterns and enrichments to be similar
161 across these two independent, large scale scRNAseq studies, supporting the general trends observed with
162 the MouseBrain dataset.

163 To gain insight into the networks of ZDHHC enzymes that might work together to coordinate *S*-
164 palmitoylation in different cell types we performed co-expression analysis (Spearman correlation)
165 between ZDHHC genes across all 265 metacell types in the MouseBrain dataset (Figure 1D; Table S2).
166 Neuron enriched *Zdhhc3*, *Zdhhc8*, *Zdhhc17* and *Zdhhc21* formed the strongest network of co-expression
167 associations, while glial cell enriched *Zdhhc2, Zdhhc9* and *Zdhhc20* formed less robust correlations with
168 other ZDHHCs. Weaker correlations were observed across the 565 cell-types in the DropViz dataset, which
169 may reflect the absence of the PNS neurons and glia in this study (Figure S1D; Table S2).

170 In order to create a list of potential substrates for the ZDHHCs in the mouse nervous system, we
171 expanded our co-expression analysis to include all expressed genes from the 'MouseBrain' dataset that
172 had significant correlation (R > 0.7) with one or more ZDHHC. We identified 914 genes that were
173 significantly correlated with DHHCs. This list was cross-referenced with the mouse SwissPalm database of
174 *S*-palmitoylated substrates identified in at least one palmitoyl-proteome or experimentally validated
175 (SwissPalm annotated; Blanc et al., 2015, 2019). We found that genes that showed correlated expression
176 with a ZDHHC were significantly enriched with *S*-palmitoylation substrates, indicating that ZDHHCs are
177 more likely to be co-expressed with their *S*-palmitoylation substrates in the brain (Figure 1E; Table S3).
178 Co-expression analysis of the 'DropViz' dataset revealed a similar enrichment of S-palmitoylation
179 substrates co-expressed with ZDHHCs (Figure S1E; Table S4), supporting the notion of ZDHHC enzyme-
180 substrate co-expression. PANTHER GO analysis of the 'MouseBrain' curated ZDHHC co-expressed *S*-
181 palmitoylation substrates revealed several significant enrichments in GO terms for biological processes
182 related to protein localization (Figure 1F), as well as enrichments for cellular components that included
183 synapses, membrane-bounded organelles, endomembranes and vesicles (Figure S2B). These findings are
184 consistent with the known role of *S*-palmitoylation in regulating protein localization and signaling
185 complexes at cellular membranes.

186 **Heterogeneity in ZDHHC expression within excitatory neurons of the dorsal hippocampus**

187 The hippocampus is a heavily studied brain region that is critical for learning and memory (Bird
188 and Burgess, 2008). A recent pooled-cell RNAseq study of excitatory neurons in the hippocampus revealed
189 extensive regional variability in gene expression profiles of the hippocampal tri-synaptic loop
190 (hipposeq.janelia.org; Cembrowski et al., 2016). In order to clearly visualize if ZDHHC expression also
191 varied in these different cell populations, we projected log transformed expression heatmaps generated
192 in BrainPalmSeq for the 'hipposeq' dorsal-ventral excitatory neuron dataset on to anatomical maps of the
193 dorsal hippocampus (Figure 2A). We observed considerable heterogeneity in the regional expression
194 patterns of the ZDHHCs. Hierarchical clustering analysis revealed that the ZDHHCs could be grouped into
195 those that showed similar expression in all regions, those that were dentate gyrus granule cell (DG)
196 enriched, DG depleted or CA1/CA2 enriched (Figure 3B). We generated comparative heatmaps for several
197 scRNAseq studies curated in BrainPalmSeq that also quantified the hippocampal excitatory neuron
198 transcriptome and found similar cross-study expression patterns for many of the ZDHHCs (Figure S3A).
199 Furthermore, *in situ* hybridization data from the Allen Institute showed a high degree of overlap with the
200 'hipposeq' derived ZDHHC expression patterns, supporting the replicability of the expression patterns
201 observed in the 'hipposeq' dataset (Figure S3B; Table S5).

202 We next sought to utilize the 'hipposeq' dataset to determine if there might be regional
203 differences in the expression of *S*-palmitoylation substrates in excitatory neurons of the dorsal
204 hippocampus, which may be potential substrates for regionally enriched ZDHHC enzymes. To investigate
205 the regionally-enriched predicted hippocampal palmitoylome, we utilized the enrichment analysis tools
206 built in to hipposeq.janelia.org (see materials and methods). Neurons in each hippocampal sub-region
207 expressed unique *S*-palmitoylation substrates that were related to highly divergent functions. We found
208 for CA1 neurons, which have highest expression of *Zdhhc2*, *Zdhhc17*, *Zdhhc23* and *Zdhhc9* (Figure 3C), the
209 CA1 enriched predicted palmitoylome (Figure 3D; Table S6) generated KEGG pathways related to 'Calcium
210 signaling', 'Glutamatergic synapse' and 'Long term potentiation', supporting the known role *S*-
211 palmitoylation plays in CA1 hippocampal synaptic plasticity (Figure 3E; Ji and Skup, 2021; Matt et al.,
212 2019). The CA1 predicted palmitoylome was composed of around 46 % synaptic proteins (SynGO
213 annotated), with SynGO ontologies related to 'synaptic vesicle exocytosis' and 'synapse organization'
214 (Figure 3F; Koopmans et al., 2019). In contrast, the predicted palmitoylome of DG granule cells which have
215 the highest expression of *Zdhhc21*, *Zdhhc4*, *Zdhhc24* and *Zdhhc8* (Figure 3G, H) generated KEGG pathways
216 related to 'Ribosome', 'Cholinergic synapse' and 'Parkinson's disease' (Figure 3I). The DG predicted-
217 palmitoylome was composed of 29 % synaptic proteins (SynGO annotated), with SynGO ontologies related

218 to ‘protein translation at presynapse’ and ‘protein translation at postsynapse’, revealing a potential role
219 for palmitoylating enzymes in regulating translation in this cell-type that has not yet been studied (Figure
220 3J). Together, we have described patterns of restricted expression of ZDHHC enzymes and *S*-
221 palmitoylation substrates in the dorsal mouse hippocampus, and generated both broad and regionally-
222 enriched predicted-palmitoylomes that give insight into the role of *S*-palmitoylation in neuronal function
223 in each of these hippocampal sub-regions.

224 **Neocortical ZDHHC expression is partially segregated across cortical layers and neuronal subclasses**

225 We next examined scRNAseq datasets curated in BrainPalmSeq from the cortex, beginning with a
226 study of the primary somatosensory cortex (SSp; Zeisel et al., 2015). We projected heatmaps of pyramidal
227 excitatory neuron ZDHHC expression generated in BrainPalmSeq onto cortical layer diagrams of SSp, again
228 revealing anatomically heterogenous excitatory neuron expression patterns of several of the ZDHHC
229 transcripts. Clustering primarily grouped the enzymes according to expression levels, with *Zdhhc21*,
230 *Zdhhc17* and *Zdhhc8* having the highest relative expression (Figure 3B). *Zdhhc2*, *Zdhhc3* and *Zdhhc20*
231 expression was also high, with the remainder of the ZDHHCs having moderate to low expression. We
232 compared these expression patterns with other datasets curated in BrainPalmSeq (Figure S4A), which
233 revealed many consistent patterns of expression maintained across several independent studies. For
234 example, multiple studies reported high expression of *Zdhhc8* in cortical Layer 2/3, enrichment of *Zdhhc2*
235 in Layer 4 and elevated expression of *Zdhhc21* in all layers, particularly in Layer 5. *Zdhhc3* and *Zdhhc20*
236 were also broadly expressed in all cortical layers across studies. Similar patterns were seen in the SSp
237 region from available in situ hybridization studies from Allen Brain Institute (Figure S3B).

238 We examined expression patterns of the ZDHHC enzymes from one of the largest neuronal
239 scRNAseq studies from the isocortex performed by the Allen Brain Institute, which identified 236
240 glutamatergic and 117 GABAergic distinct neuron metacell types (Yao et al., 2021). We averaged ZDHHC
241 expression data downloaded from BrainPalmSeq for the major metacell clusters from all regions of the
242 isocortex, according to their anatomical location and/or axon projection and plotted ranked heatmaps
243 (Figure 3C,D). We again found that *Zdhhc20* was the ZDHHC transcript with the highest expression, with
244 broad expression across the majority of glutamatergic and GABAergic cell-types. Elevated expression of
245 *Zdhhc14* was found in both glutamatergic and GABAergic neurons, which was moderately expressed in
246 other studies of the brain and cortex discussed previously. Numerous subtypes of projection neurons
247 featured at the top of the ranking including pyramidal tract (PT) projecting neurons found in layer 5 of the
248 cortex, that have extensive dendritic branching and long-range axonal projections to the spinal cord,

249 brainstem and midbrain, as well as the ipsilateral cortex, striatum and thalamus. Other neuron subtypes
250 with high ZDHHC expression included a number of intratelencephalic (IT) projecting neuron classes,
251 including those from Layer 4/5 of the temporal/perirhinal/ectorhinal/entorhinal cortices, Car3 expressing
252 Layer 6 neurons, Layer 6b neurons, and Cortex IT projecting neurons from all cortical layers (Harris and
253 Shepherd, 2015; Yao et al., 2021). GABAergic neurons of the isocortex also showed elevated expression
254 of the common neuronal ZDHHCs including *Zdhhc2*, *Zdhhc3*, *Zdhhc14*, *Zdhhc17*, *Zdhhc20* and *Zdhhc21*.
255 The highest mean ranked expression was observed in the recently categorized Sncg neurons that
256 correspond to *Vip*$^+$/*Cck*$^+$ multipolar or basket cells (Tasic et al., 2018), and lowest expression was observed
257 in Vip subclass of interneurons.

258 Together, our observations reveal that the complex transcriptional diversity of neurons that has
259 recently been revealed by RNA sequencing also includes heterogeneity in the expression of the ZDHHC
260 enzymes that mediate palmitoylation. These expression patterns are likely to influence enzyme-substrate
261 interactions along with the function of *S*-palmitoylation substrates, and as such have an influence over
262 neuronal development, function and synaptic plasticity.

263 **De-palmitoylating enzyme and ZDHHC accessory protein expression in the nervous system shows**
264 **regional and cell-type specific patterning**

265 Dynamic turnover of protein *S*-palmitoylation is mediated by the activity of de-palmitoylating
266 enzymes, which determine the half-life of *S*-palmitoylation on a target protein. These include acyl-protein
267 thioesterases 1 and 2 (APT1, APT2; encoded by *Lypla1*, *Lypla2*), palmitoyl-protein thioesterase 1 (PPT1)
268 and the more recently identified α/β hydrolase domain-containing 17 proteins (ABHD17A, ABHD17B and
269 ABHD17C). Compared with the ZDHHC enzymes, relatively less is known about the substrates, sub-cellular
270 localization and brain expression patterns of this family of enzymes. We next explored BrainPalmSeq to
271 determine which cell-types/brain regions show the highest expression of de-palmitoylating enzymes.

272 We first examined expression heatmaps for the known de-palmitoylating enzymes across the 265
273 cell-types identified in the 'MouseBrain' dataset (Figure 4A) and the cell-type averages for the 565 cell-
274 types from the 'DropViz' dataset (Figure S4A). *Ppt1* and *Abhd17a* were the enzymes with the broadest
275 expression across all cell-types, with *Ppt1* expression being notably elevated in neurons of the hindbrain
276 and immune cells, and *Abhd17a* being elevated in hindbrain neurons, sensory neurons, oligodendrocytes
277 and epithelial cells. Ranked expression (sorted by averages descending) of de-palmitoylating enzymes in
278 the 'MouseBrain' (Figure 4B) and 'DropViz' (Figure 4C) ranked oligodendrocyte lineage cells among the
279 cell-types with the highest expression of de-palmitoylating enzymes overall, primarily due to elevated

280 expression of *Abhd17b*, mirroring oligodendrocyte enrichment of ZDHHC enzyme expression and again
281 indicating that dynamic regulation of *S*-palmitoylation may be particularly important in this cell type.
282 *Lypla2* expression was greater than *Lypla1* overall in the brain, with *Lypla2* expression being highest in
283 neurons and ependymal cells. *Abhd17c* had the lowest brain expression of all the de-palmitoylating
284 enzymes studied. Correlation analysis between the ZDHHCs and de-palmitoylating enzymes revealed
285 numerous instances of co-expression with almost every ZDHHC (Figure 4D), revealing potential
286 cooperative pairs of palmitoylating and de-palmitoylating enzymes in the nervous system.

287 Although the ZDHHC enzymes are thought to have the ability to act autonomously, several
288 accessory proteins have been discovered that can regulate ZDHHC stability, localization and catalytic
289 activity (Salaun et al., 2020). These include GOLGA7 (GCP16), which can bind to ZDHHC9 enhancing both
290 protein stability and increasing enzymatic activity by stabilizing the ZDHHC9 auto-palmitoylated
291 intermediate that is formed prior to palmitate transfer to the substrate protein (Mitchell et al., 2014;
292 Swarthout et al., 2005). Both GOLGA7 and related isoform GOLGA7B are also able to interact with
293 ZDHHC5, with the latter having an influence on ZDHHC5 plasma membrane localization (Woodley and
294 Collins, 2019). Finally, SELK (SELENOK; Selenoprotein K) is an ER localized protein that was found to
295 interact with ZDHHC6, stabilize the auto-palmitoylated intermediate and increase palmitoylation of
296 substrate proteins including the IP_3 receptor (Fredericks et al., 2017, 2014).

297 Widespread expression of *Selk* was observed across all cell-types, with expression being
298 considerably higher than any of the ZDHHCs, de-palmitoylating enzymes or other accessory proteins
299 (Figure 4A, S4A). This is consistent with the known functions of SELK in the ER associated protein
300 degradation pathway and regulation of ER calcium flux (Pitts and Hoffmann, 2018). *Golga7b* expression
301 was widespread across neuronal subtypes but barely detected in glial cells (Figure 4A, S4A). Accordingly,
302 *Golga7b* expression was also strongly correlated with several of the ZDHHCs that were most highly
303 expressed in neurons, including *Zdhhc3*, *Zdhhc8*, *Zdhhc17* and *Zdhhc21* (Figure 4D). In contrast, *Golga7*
304 was enriched in glial cells, particularly in oligodendrocytes, similar to ZDHHC9 for which GOLGA7 is a key
305 accessory protein (Figure 44A, S4A). GOLGA7 and GOLGA7B share 61% amino acid similarity, but their
306 expression was either not correlated or negatively correlated (Table S2), indicating that the ZDHHC
307 association of each of these proteins may be regulated in part by differential expression.

308 **Loss of function mutations in palmitoylating and de-palmitoylating**

309 Impaired regulation of *S*-palmitoylation has been implicated in numerous neurological disorders,
310 many of which are due to loss of function (LOF) mutations in palmitoylating and de-palmitoylating

311 enzymes (Cho and Park, 2016; Matt et al., 2019). We next sought to determine if the regional and cell
312 type expression data available in BrainPalmSeq could reveal insights into the pathogenesis of disorders
313 caused by LOF mutations in palmitoylating and de-palmitoylating enzymes. As many of these diseases
314 have a neurodevelopmental origin, we examined whole brain datasets curated in BrainPalmSeq from the
315 neonatal (Rosenberg et al., 2018), adolescent (Zeisel et al., 2018) and adult (Sjöstedt et al., 2020) mouse
316 brain.

317 A single nucleotide polymorphism (SNP) in the *ZDHHC8* gene has been implicated in increased
318 susceptibility to schizophrenia (Chen et al., 2004; Mukai et al., 2004), while hemizygous microdeletion in
319 the chromosomal locus 22q11, which encodes a number of genes including *ZDHHC8*, is one of the highest
320 known genetic risk factors to developing schizophrenia (Figure 5A; Karayiorgou et al., 2010). To assess the
321 developmental expression of *Zdhhc8*, we averaged expression within broadly defined cell-type clusters
322 that could be applied to both the Rosenberg and Zeisel scRNAseq datasets (Figure 5A, B; Table S7). *Zdhhc8*
323 expression was highest in neurons of the cortex and hippocampus, followed by neurons of the mid- and
324 hindbrain at both developmental ages. To explore regional expression in the adult mouse brain, we
325 projected BrainPalmSeq generated heatmaps expression data from the 'Protein Atlas' mouse whole brain
326 dataset (bulk RNAseq from 13 brain regions) onto anatomical maps of the mouse brain, again revealing
327 highest expression of *Zdhhc8* in the cortex, followed by the hippocampus and basal ganglia (Figure 5C;
328 Sjöstedt et al., 2020). *Zdhhc8* expression was particularly enriched in Layer 2/3 of the neonatal (not shown)
329 and adult mouse cortex (Figure S3B), which is the cortical layer with the most pronounced morphological
330 deficits in patients with Schizophrenia (Glantz and Lewis, 2000; Kolluri et al., 2005; Wagstyl et al., 2016).
331 Together, we found *Zdhhc8* expression patterns in the mouse brain that are established early in postnatal
332 development and maintained into adulthood, that also overlay with many brain regions and cell types
333 that are known to be severely affected in patients with schizophrenia. These observations support a model
334 in which LOF *ZDHHC8* mutations may elicit many of the symptoms of schizophrenia by disrupting *S*-
335 palmitoylation and normal neuronal development in these brain regions.

336 Mutations in the *ZDHHC9* gene, which is located on the X chromosome, have been identified in
337 ~2% of X-linked intellectual disability (ID) patients (Raymond et al., 2007; Tzschach et al., 2015).
338 Neuroanatomical abnormalities reported in patients with *ZDHHC9* mutations include decreased cortical,
339 thalamic and striatal volume, and widespread white matter abnormalities with prominent hypoplasia
340 (under-development) of the corpus callosum (Baker et al., 2015; Bathelt et al., 2016). Disrupted white
341 matter integrity is thought to underlie deficits in global and local brain connectivity in patients with

342 *ZDHHC9* mutations (Bathelt et al., 2017). *Zdhhc9* knock-out mice also develop similar pathological
343 changes, including decreased volume of the corpus callosum (Kouskou et al., 2018). We observed
344 considerable cell-type enrichment of *Zdhhc9* in oligodendrocytes across studies and developmental ages
345 (Figure 5D, E), accompanied by moderate neuronal expression of *Zdhhc9* relative to other ZDHHCs across
346 several brain regions including the hippocampus and cortex (Figure 2A, 3A, 5D, E), consistent with the
347 known function of ZDHHC9 in regulating neuronal development (Shimell et al., 2019). Regionally, we
348 found *Zdhhc9* expression in adult mice to be highly enriched in the corpus callosum, the largest white
349 matter tract in the brain (Figure 5F). As myelin production by oligodendrocytes is critical for maintaining
350 white matter integrity, these observations indicate that disrupting *S*-palmitoylation in oligodendrocytes
351 may underlie the white matter pathology and decreased connectivity observed in patients with X-linked
352 ID and *ZDHHC9* mutations.

353 Infantile neuronal ceroid lipofuscinosis (INCL or CLN1 disease) is a severe neurological disorder
354 caused by LOF mutations in the *PPT1* gene that presents in the first 6 - 12 months of life and is
355 characterized by rapid developmental regression, blindness and seizures, with continual deterioration
356 until death in early childhood (Nita et al., 2016). While PPT1 is thought to primarily localize to lysosomes
357 with an essential role in lysosomal degradation of *S*-palmitoylated proteins (Lu et al., 1996), PPT1 also has
358 a synapse-specific function in regulating synaptic vesicle cycling and synaptic transmission (Koster and
359 Yoshii, 2019). We found that neuronal *Ppt1* expression was high in postnatal neurons of the spinal cord,
360 olfactory bulb and mid/hindbrain, while microglia were the highest expressing non-neuronal cell type at
361 both postnatal ages (Figure 5G, H). Neurodegeneration has been detected in the spinal cord prior to their
362 onset within the brain in *Ppt1* knock-out mice, accompanied by extensive glial cell activation including
363 microgliosis, which is a pathological hallmark of CLN1 disease (Shyng et al., 2017). Mid-/hindbrain neurons
364 also had high expression of *Ppt1,* consistent with reports that *Ppt1* knock-out mice show earliest signs of
365 brain pathology in the thalamus (Kielar et al., 2007). Overall, we observed widespread *Ppt1* expression in
366 almost every brain region in adult mice, consistent with the sweeping neurological deficits associated with
367 CLN1 disease (Figure 5I). Together, these observations reveal how the loss of *Ppt1* in cell types with high
368 *Ppt1* expression may lead to cell death/dysfuntion in the early stages of CLN1 disease.

369 **ZDHHC cell type enrichments can be used to predict and validate ZDHHC substrates**

370 We next tested if ZDHHC expression patterns identified from BrainPalmSeq could be used to
371 predict and validate *S*-palmitoylation substrates for regionally enriched ZDHHCs. We focused on *Zdhhc9*,
372 which showed a consistent cell-type enrichment in oligodendrocytes across multiple studies in

373 BrainPalmSeq, while LOF mutations in *ZDHHC9* are known to result in decreased white matter integrity in
374 the brain (Raymond et al., 2007). Examination of the Marques et al oligodendrocyte-specific scRNAseq
375 dataset curated in BrainPalmSeq revealed that oligodendrocyte *Zdhhc9* expression increased throughout
376 maturation, with highest expression in the myelin forming (MFOL) intermediate-maturity subtype
377 oligodendrocytes, and slightly lower expression maintained in mature oligodendrocytes (MOL; Figure 6A;
378 Marques et al., 2016).

379 To identify potential substrates for ZDHHC9, we cross-referenced a list of MFOL/MOL enriched
380 genes identified in the study by Marques et al (Marques et al., 2016) with the SwissPalm database to
381 identify known palmitoylation substrates in these cell types (Swiss Palm Annotated; Table S8, Figure 6B;
382 Blanc et al., 2019, 2015). PANTHER analysis of cellular component enrichments for these substrates
383 revealed the most significant enrichment was for the term 'myelin sheath' (30 proteins; Figure 6C, S6). To
384 determine if any of the myelin sheath associated proteins could be palmitoylated by ZDHHC9, we selected
385 three proteins (MOBP, PLP1 and CNP) for experimental validation (Figure 6C). We expressed either of
386 these candidate substrates together with ZDHHC9 and its accessory protein GOLGA7 in HEK293T cells, and
387 determined the proportion of palmitoylated substrate using an Acyl-Rac palmitoylation assay (Forrester
388 et al., 2011). In this assay, free cysteine residues of cell lysates were first blocked, followed by cleavage of
389 the palmitoyl-thioester bond with hydroxylamine, resulting in the exposure of a free sulfhydryl group.
390 Cleaved lysates were then applied to a sepharose resin to capture palmitoylated proteins containing a
391 free sulfhydryl group. Un-bound proteins (Unpalm Fraction) were first extracted from the resin mixture,
392 followed by elution of bound palmitoylated proteins from the resin (Palm Fraction). To assess non-specific
393 binding of unpalmitoylated protein to the resin, half of the cell lysate was processed without the cleavage
394 step (NSB control). Co-expression of HA-ZDHHC9 and FLAG-GOLGA7 increased the palmitoylated fraction
395 of MOBP and PLP1, revealing that these proteins are substrates for ZDHHC9 (Figure 6D, E, G). Conversely,
396 CNP was not identified as a ZDHHC9 substrate in our assay (Figure 6F. G). These results reveal how the
397 cell-type enrichments of ZDHHC enzymes identified in this study can be used, along with the lists of
398 similarly enriched palmitoylation substrates, to guide the identification of enzyme-substrate interactions
399 that can be further investigated *in vivo*.

400

401 **Discussion**

402 **BrainPalmSeq as a tool to generate hypotheses about proteins that control S-palmitoylation in the**
403 **brain**

404 We have demonstrated the utility of BrainPalmSeq by providing examples of how this database
405 can be used to explore detailed region and cell type-specific expression patterns of the known
406 palmitoylating and de-palmitoylating enzymes, and their accessory proteins. We reveal how these
407 expression patterns can be used to predict/validate *S*-palmitoylation substrates and better understand
408 diseases associated with loss of function mutations in the enzymes that mediate *S*-palmitoylation. Given
409 the number of brain regions and cell types incorporated into BrainPalmSeq that were not discussed in the
410 present study, including the thalamus, hypothalamus, amygdala, striatum and cerebellum, there is rich
411 potential for users to explore the data and generate hypotheses about the role of these enzymes in the
412 brain.

413 **Insights into the role of *S*-palmitoylation associated enzymes in brain physiology and pathology**

414 While we found that many of the proteins we studied showed correlated expression across the
415 entire mouse nervous system, particularly those enriched in neurons including *Zdhhc3*, *Zdhhc8*, *Zdhhc17*
416 and *Zdhhc21*, expression of these genes was segregated within more narrowly defined neuronal
417 populations such as the excitatory pyramidal neurons within the hippocampal tri-synaptic loop or layers
418 of the somatosensory cortex. This is in line with the extensive neuronal transcriptional heterogeneity
419 identified recently by a number of scRNAseq studies (Saunders et al., 2018; Yao et al., 2021; Zeisel et al.,
420 2015, 2018). The genes that determine neuronal identity fall under four broad functional categories: those
421 that control transcriptional programs, membrane conductance, neurotransmission, and synaptic
422 connectivity (Zeisel et al., 2018). We report also heterogeneity in the neuronal fingerprint of
423 palmitoylating and de-palmitoylating enzyme expression, which will in turn give rise to differential *S*-
424 palmitoylation of neuronal proteins. Future work is needed to determine how these specific ZDHHC
425 expression patterns are related to dynamic *S*-palmitoylation in these neuronal sub-types, and how the
426 elevated expression of certain ZDHHCs can alter neuronal function. Given that *S*-palmitoylation is key
427 regulator of neuronal development, and that nearly half of all known synaptic proteins are substrates for
428 palmitoylation (Sanders et al., 2015), this heterogeneity is likely to be a key mechanism in the fine tuning
429 of neuronal function and synaptic transmission.

430 Many of the ZDHHCs that we observed with consistently elevated expression across multiple
431 studies in BrainPalmSeq have already been studied in the context of neuronal signaling, including ZDHHC2,

432 ZDHHC3, ZDHHC8 and ZDHHC17 (Ji and Skup, 2021; Matt et al., 2019). In contrast, ZDHHC20 and ZDHHC21
433 are relatively understudied in the nervous system, despite our observation that these are two of the most
434 abundantly expressed ZDHHCs across neuronal cell types, with broad expression of *Zdhhc20* also in glial
435 cells. A recent study defined a role for ZDHHC21 in the palmitoylation of serotonergic receptor 5-HT1A
436 and implicated downregulation of ZDHHC21 in the development of major depressive disorder (Gorinski et
437 al., 2019). Interestingly, both ZDHHC20 and ZDHHC21 have a potential role in the pathogenesis of
438 Alzheimer's disease, as they can palmitoylate BACE1, Tau and amyloid precursor protein (Cho and Park,
439 2016). More work is needed to understand the likely important role of these enzymes in the brain.

440 We made several other interesting observations during our examination of BrainPalmSeq that
441 were not discussed in detail in the present study but we believe warrant further investigation. For
442 example, the particularly elevated expression of *Zdhhc2* in peripheral sensory neurons may indicate an
443 important role for palmitoylation in this cell type. Across multiple studies we observed striking enrichment
444 of *Zdhhc14* in cerebellar Purkinje neurons, a cell type in which *S*-palmitoylation is known to be important
445 for long-term depression, although the role of ZDHHC14 in this process has not yet been investigated
446 (Thomas et al., 2013). *Zdhhc23* was similarly enriched in the CA2 region of the hippocampus, with
447 comparatively low expression across other cell types. More broadly, the elevated expression of a variety
448 of palmitoylating enzymes in neurons that utilize acetylcholine or monoamines as neurotransmitters
449 would suggest an important role for *S*-palmitoylation in these neurons that has yet to be explored.
450 Accordingly, many of the key proteins involved in cholinergic synaptic transmission are *S*-palmitoylation
451 substrates including muscarinic acetylcholine receptor M2 (CHRM2), acetylcholinesterase (ACHE) and
452 ATP-citrate synthase (ACLY; Blanc et al., 2015, 2019). Our observations of co-enrichment of certain
453 palmitoylating and de-palmitoylating enzymes are also of interest, such as *Abhd17b* and *Zdhhc9* in
454 oligodendrocytes. It is possible that these enzymes share substrates to mediate dynamic palmitoylation,
455 or have separate substrates in order to maintain stable *S*-palmitoylation states of certain oligodendrocyte
456 expressed proteins. Importantly, the data accessibility in BrainPalmSeq will enable researchers to develop
457 hypotheses regarding their cell type, brain region or protein of interest.

458 The palmitoylome of each cell type in the nervous system is likely to be highly heterogeneous and
459 will be determined by the expression of both the *S*-palmitoylation substrates and the palmitoylating and
460 de-palmitoylating enzymes in a given cell type. Furthermore, accumulating evidence has revealed that
461 this palmitoylome can be altered by extrinsic factors such as chronic stress and neuronal activity (Kang et
462 al., 2008; Zareba-Koziol et al., 2019). While we have provided predicted palmitoylomes composed of

463 several highly expressed or enriched *S*-palmitoylation substrates in select brain regions and cell types,
464 experimental validation to reveal the relative palmitoylation of substrates under various conditions is
465 needed to fully understand these cellular differences. Nevertheless, we were able utilize our predicted
466 palmitoylomes to validate substrates for ZDHHC9, giving insight into the potential role of this enzyme in
467 myelin regulation in the brain.

468 Neurological disorders that arise from LOF gene mutations might be predicted to lead to
469 pathological changes that are more severe in the brain regions in which these genes are most highly
470 expressed. We observed this type of regional overlay for the expression patterns of *Zdhhc8*, *Zdhhc9* and
471 *Ppt1*. Numerous other brain disorders are thought to be exacerbated by an imbalance in *S*-palmitoylation,
472 such as decreased *S*-palmitoylation of HTT in huntington's disease (Virlogeux et al., 2021; Yanai et al.,
473 2006), increased *S*-palmitoylation of APP and TAU in Alzheimer's disease (Cho and Park, 2016), and
474 decreased *S*-palmitoylation of 5-HTA receptor in major depressive disorder (Gorinski et al., 2019). Efforts
475 are already underway to normalize aberrant palmitoylation in neurological diseases in order to improve
476 clinical outcomes (Roberts et al., 2012; Virlogeux et al., 2021). Understanding the brain expression
477 patterns of the enzymes that mediate palmitoylation in these diseases will be key to developing and
478 targeting such therapeutics.

479 **Differential gene expression as a means to control *S*-palmitoylation in the brain**

480 The mechanisms that govern ZDHHC enzyme-substrate interactions are complex and still not fully
481 understood. While the majority of post-translational modifications including phosphorylation and N-
482 glycosylation are highly sequence specific (Schwarz and Aebi, 2011; Ubersax and Ferrell, 2007), several
483 studies have revealed that *S*-palmitoylation by ZDHHCs can be stochastic, proximity based and lacking in
484 stereo-selectivity (Rocks et al., 2010; Rodenburg et al., 2017). Contrasting studies have shown that
485 numerous ZDHHCs have specific protein interacting domains including ankyrin repeat (AR), PDZ and SH3
486 domains that facilitate substrate interactions, providing support for a model in which more specific
487 enzyme-substrate interactions can govern *S*-palmitoylation (Abrami et al., 2017; Lemonidis et al., 2015;
488 Plain et al., 2020; Rana et al., 2018; Thomas et al., 2012; Verardi et al., 2017). Furthermore, a recent study
489 found striking substrate specificity for several ZDHHCs with the G-protein subunit Gαo, and revealed
490 intriguing observations that the subcellular localization of a number of *S*-palmitoylation substrates could
491 be controlled by changing the localization, and importantly, the expression of certain ZDHHC enzymes. In
492 this study, *S*-palmitoylated substrates accumulated in the subcellular compartment in which their partner
493 ZDHHCs were targeted (Solis et al., 2020). This is particularly relevant as the ZDHHCs are known to have

494 diverse subcellular localizations including the golgi, ER, endosomes and plasma membrane (Globa and
495 Bamji, 2017). Transcriptional control of differentially compartmentalized palmitoylating and de-
496 palmitoylating enzymes could therefore be an essential mechanism for regulating the subcellular
497 localization, and function, of *S*-palmitoylated protein substrates. Accordingly, LOF mutations in certain
498 ZDHHC enzymes leads to cell type-specific disruption in *S*-palmitoylation that is not compensated by other
499 members of the large ZDHHC family. We provide a means to investigate the expression of the proteins
500 that mediate *S*-palmitoylation, making BrainPalmSeq an invaluable resource to both researchers and
501 clinicians that are working to better understand the role of *S*-palmitoylation in the brain.

502

503 **Supplementary Tables**
504 https://docs.google.com/spreadsheets/d/1egtQL5tY5WolePrv2757Mxwrkcm1hc5gQycOvmsvKdk/edit?u
505 sp=sharing

506

507 **Figure Legends**

508 **Figure 1. Heterogeneous ZDHHC expression in the mouse nervous system**

509 (A) Heatmap showing expression for the 24 ZDHHC genes, extracted from scRNAseq study of mouse CNS
510 and PNS (Zeisel et al., 2018). Each column represents one of the 265 metacells classified in the study.
511 Metacells are organized along x-axis according to hierarchical clustering designations generated by Zeisel
512 et al. Full metadata for this study available on BrainPalmSeq.

513 (B) Heatmap showing mean ZDHHC expression per hierarchical cluster, with columns and rows sorted by
514 descending mean ZDHHC expression per row/column.

515 (C) Heatmap showing mean ZDHHC expression per neurotransmitter cluster for all PNS and CNS neurons.
516 Columns and rows are sorted as in B.

517 (D) Correlation network showing ZDHHC co-expression across all metacells in 'MouseBrain' (Spearman R
518 > 0.5). Numbers in nodes correspond to ZDHHC number. Node color represents mean expression across
519 all metacells. Edge thickness represents strength of correlation.

520 (E) Graph showing proportion of genes from 'MouseBrain' dataset that are co-expressed with one or more
521 ZDHHC and also substrates for *S*-palmitoylation (SwissPalm annotated). 'Brain expressed' = 15,389 protein
522 coding genes expressed in the postnatal mouse brain, curated from the MGI RNAseq studies database. 'R
523 > 0.7 ZDHHC co-expressed' = 914 genes co-expressed with one or more ZDHHC (Spearman R > 0.7). 'R >
524 0.8 ZDHHC co-expressed' = list of 167 genes co-expressed with one or more ZDHHC (Spearman R > 0.8).
525 Brain expressed vs. R > 0.7: $p < 0.001$; R > 0.7 vs R > 0.8: $p < 0.01$; Fisher's exact test.

526 (F) Graph of GO biological process analysis. Gene IDs from the 'MouseBrain' dataset (Zeisel et al., 2018)
527 that showed correlated expression with one or more ZDHHC (R > 0.7) and were also Uniprot reviewed and
528 SwissPalm annotated were used as input.

529 Units for all heatmaps in figure: mean log2(counts per 10,000 + 1).

530 **Figure 2. Diversity in ZDHHC expression and S-palmitoylation substrate expression in the hippocampus**

531 (A) Heatmap of excitatory neuron ZDHHC expression from dorsal hippocampus (original pooled cell
532 RNAseq data from Cembrowski et al., 2016) projected onto diagrams of dorsal hippocampus.

533 (B) Hierarchical clustering of ZDHHC expression data in A.

534 (C) Heatmap showing top 6 ranked expressing ZDHHCs in dorsal CA1 in descending order.

535 (D) Pie chart showing proportion genes with enriched expression in dorsal CA1 (dCA1) that are also
536 substrates for palmitoylation (SwissPalm annotated).

537 (E) KEGG analysis of the dCA1 enriched/SwissPalm annotated genes.

538 (F) SynGO analysis of the dCA1 enriched/SwissPalm annotated genes.

539 (G-J) As in (C)-(F) but for the dorsal dentate gyrus (dDG).

540 Heatmap legend in (A) applies to all heatmaps (logFKPM).

541 **Figure 3. Pyramidal neuron layer specific ZDHHC expression**

542 (A) Heatmap of excitatory neuron ZDHHC expression from somatosensory cortex (original data scRNAseq
543 data from Zeisel et al., 2015) projected onto diagrams of cortical layers.

544 (B) Hierarchical clustering of ZDHHC expression data in A. Heatmap units in (A, B): mean log2(counts per
545 10,000 + 1)

546 (C) Heatmap of scRNAseq data from Allen Brain 10X genomics (Yao et al., 2021). Data are represented as
547 mean ZDHHC expression per excitatory neuron subtype, with columns and rows sorted by descending
548 mean ZDHHC expression per row/column.

549 (D) As in (C) but for inhibitory neuron subtypes. Heatmap units for (C, D):

550 **Figure 4. Heterogeneous de-palmitoylating enzyme and ZDHHC accessory protein expression in the**
551 **mouse nervous system**

552 (A) Heatmap showing expression of de-palmitoylating enzymes (top) and ZDHHC accessory subunits
553 (bottom), extracted from scRNAseq study of mouse CNS and PNS (Zeisel et al., 2018). Each column
554 represents one of the 265 metacells classified in the study. Metacells are organized according to
555 hierarchical clustering designations generated by Zeisel et al.

556 (B) Heatmap showing mean de-palmitoylating enzyme expression per hierarchical cluster, with columns
557 and rows sorted by descending mean ZDHHC expression per row/column.

558 (C) As B but for ZDHHC accessory proteins.

559 (D) Correlation network showing ZDHHC co-expression with de-palmitoylating enyzmes and accessory
560 proteins across all metacells in 'MouseBrain' (Spearman R > 0.4). Node color represents mean expression
561 across all metacells. Edge thickness represents strength of correlation.

562 **Figure 5. Disease associated palmitoylating enzyme regional and cell-type expression overlays with**
563 **brain pathology in associated LOF disorders**

564 (A) Heatmap showing ranked *Zdhhc8* expressing neuronal and glial cell types in descending order. Original
565 data from scRNAseq neonatal mouse brain study; Rosenberg et al., 2018. Cell types were averaged as
566 described in Table SY. Heatmap units: log2(TPM+1).

567 (B) As in A but original data from scRNAseq adolescent mouse brain study Zeisel et al (2018). Heatmap
568 units: mean log2(counts per 10,000 + 1).

569 (C) Heatmap of *Zdhhc8* expression from whole brain regional bulk RNAseq data (original data from
570 'Protein Atlas'; Sjöstedt et al., 2020) projected onto anatomical map of mouse brain. Heatmap units:
571 FKPM.

572 (D-F) As in (A)-(C) but for *Zdhhc9*.

573 (G-I) As in (A)-(C) but for *Ppt1*.

574 **Figure 6. Validation of predicted *S*-palmitoylation substrates of *Zdhhc9* derived from cell-type**
575 **enriched expression**

576 (A) Graph of expression data for *Zdhhc9* extracted from BrainPalmSeq. Original data from oligodendrocyte
577 scRNAseq study by Marques et al. Expression units: mean log2(counts per 10,000 + 1).

578 (B) Diagram illustrating workflow to generate a list of oligodendrocyte enriched palmitoylation
579 substrates, GO annotated for myelin sheath for experimental validation.

580 (C) STRING diagram of myelin sheath annotated palmitoylation substrates.

581 (D) Western blot following Acyl-RAC palmitoylation assay in HEK293 cells to identify palmitoylated and
582 unpalmitoylated fractions of FLAG-MOBP either without or with co-transfection of FLAG-GOLGA7 and
583 HA-ZDHHC9. Input = unprocessed protein lysate. NSB control = non-specific binding of unpalmitoylated
584 protein to sepharose resin in control pipeline. Palm fraction = palmitoylated protein (bound to
585 sepharose resin). Unpalm fraction = unpalmitoylated protein (did not bind to sepharose resin).

586 (E-F) As in (D) but for FLAG-PLP1 or FLAG-CNP.

587 (G) Graphs quantifying the ratio of palmitoylated to unpalmtoylated protein either with or without co-
588 transfections with FLAG-GOLGA7 and HA-ZDHHC9. n = 4-6 cultures per condition. $**$ $p < 0.01$, $***$ $p <$
589 0.001; two-way ANOVA; Šídák's post hoc; mean ± SEM.

590

Materials and Methods

Data processing for BrainPalmSeq

For Zeisel et al., 2018 ('MouseBrain'), single-cell counts (UMI from 3' end counting) were downloaded from MouseBrain.org (loom file named l5_all.loom), and log normalized by first scaling the expression values provided to a sum of 10,000 per cell before calculating log2(scaled_counts+1). Averages were then performed by brain region, neurotransmitter and taxonomy for each gene.

For DropVIz Metacell counts were downloaded from DropViz.org (count file metacells.BrainCellAtlas_Saunders_version_2018.04.01.RDS and annotation file annotation.BrainCellAtlas_Saunders_version_2018.04.01.RDS) and log normalized by first scaling the expression values provided to a sum of 10,000 per metacell before calculating log2(scaled_counts+1). Averages were then performed by cell type, tissue and class for each gene. Genes associated with palmitoylation were selected in order to create the heatmaps.

For Zeisel, Single-cell counts (UMI from 3' end counting) were downloaded from https://storage.googleapis.com/linnarsson-lab-www-blobs/blobs/cortex/expression_mRNA_17-Aug-2014.txt, and log normalized by first scaling the expression values provided to a sum of 10,000 per cell before calculating log2(scaled_counts+1). Averages were then performed by cluster, tissue and class for each gene. Genes associated with palmitoylation were selected in order to create the heatmaps, categories comprising fewer than 5 single cells are not displayed.

Marques, Single-cell counts (UMI from 3' end counting) were downloaded from GEO with accession ID GSE75330 (file GSE75330_Marques_et_al_mol_counts2.tab) and log normalized by first scaling the expression values provided to a sum of 10,000 per cell before calculating log2(scaled_counts+1). Averages were then performed by cluster and region for each gene. Genes associated with palmitoylation were selected in order to create the heatmaps, categories comprising fewer than 5 single cells are not displayed.

For Rosenberg single-cell counts (UMI from 3' end counting) were downloaded from GSE110823, and log normalized by first scaling the expression values provided to a sum of 10,000 per cell before calculating log2(scaled_counts+1). Averages were then performed by brain region, neurotransmitter and taxonomy for each gene. Genes associated with palmitoylation were selected in order to create the heatmaps.

Data from Sjöstedt el al. were downloaded as Protein-coding transcripts per million (pTPM) from proteinatlas.org ("RNA mouse brain region gene data") and not further processed.

For Hipposeq, expression data were downloaded as FKPM directly from hipposeq.janelia.org and were not further processed.

For Allen Brain 10X data, expression data were downloaded as trimmed means (25%-75%) Log2(CPM+1) from portal.brain-map.org/ and were not further processed.

Correlation analysis

Spearman correlation values between genes and their significances were calculated in R using the expression results obtained for each cell type as described above.

627 **Identification of *S*-palmitoylation substrates with SwissPalm**

628 Gene lists were inputted into SwissPalm (https://swisspalm.org/proteins) input file function and cross-
629 referenced with 'Dataset 3: Palmitoylation validated or found in at least one palmitoyl-proteome
630 (SwissPalm annotated)' for Mus Musculus, with an additional filter for UniProt 'Reviewed' proteins.

631 **Generating a predicted palmitoylome for dorsal hippocampus**

632 To curate the regionally enriched predicted-palmitoylome, the enrichment analysis tools in hipposeq
633 (https://hipposeq.janelia.org/) were used to compare each of the selected Cell Lines vs the other Cell Lines
634 in the analysis (Selected Cell Lines = dorsal DG, CA3, CA2 and CA1), with the following parameters: 'Fold
635 threshold' = 1.5; 'FKPMmin threshold' = 5, 'FDR' = 0.05. The resulting lists of regionally enriched transcripts
636 were cross referenced with SwissPalm as described above to identify regionally enriched *S*-palmitoylation
637 substrates.

638 **Bioinformatic analysis**

639 Gene Ontology (GO) analysis was performed using statistical overrepresentation tests in PANTHER16.0
640 (Mi et al., 2009) with default settings and mus musculus as the reference species. Biological process GO
641 terms were extracted and ranked according to false discovery rate (FDR). Kyoto Encyclopedia of Genes
642 and Genomes (KEGG) analysis was performed using the web-based program Enrichr (Chen et al., 2013;
643 Kuleshov et al., 2016) and ranked according to -log Adjusted P-value. Synaptic Gene Ontologies (SynGO;
644 version 1.1) analysis was performed using default settings with brain expressed genes as a background
645 and and terms for 'biological process' were ranked according to -log Adjusted P-value. Functional protein
646 interaction networks were identified using the Search Tool for the Retrieval of Interacting Genes (STRING)
647 11.0 (Szklarczyk et al., 2019) with mus musculus as the reference species. Seven types of protein
648 interactions were used for network generation, including text mining, neighborhood, co-occurrence, co-
649 expression, gene fusion, experiments and databases.

650 **Data presentation**

651 Heatmaps were plotted and hierarchical clustering performed in Displayr (https://www.displayr.com)
652 using the 'Dendrogram' function. Cytoscape (Version 3.8.0) was used to draw correlation networks.

653 **Heatmap creation for BrainPalmSeq**

654 All plots for the BrainPalmSeq database were generated using curated RNA sequencing datasets. Python
655 3 and Javascript scripts were used with the plotting library Bokeh to generate the interactive heatmaps to
656 display and compare these datasets on the BrainPalmSeq website (Bokeh Development Team, 2018).

657 **Cell culture**

658 HEK293T cells were thawed and aliquoted into a 10cm dish with 10mL prewarmed (37°C) DMEM
659 (GIBCO, Thermo Fisher Scientific, Waltham, MA) supplemented with 10% fetal bovine serum (FBS)
660 (GIBCO, Thermo Fisher Scientific, Waltham, MA) and 1% Pen/Strep(P/S) (GIBCO, Thermo Fisher
661 Scientific, Waltham, MA). HEK293T cells were then placed in a 37°C incubator with 5% CO2 and
662 passaged approximately every 5 days, or once confluency was achieved.

663 **Transfection**

664 70%-80% confluent HEK293T cells were transfected using Lipofectamine 2000 (Invitrogen/Life
665 Technologies, Carlsbad, CA) according to the manufacturer's recommendations. Each well of a 6-well
666 plate was transfected with a total of 3ug DNA, 150uL of Opti-Mem (GIBCO, Thermo Fisher Scientific,
667 Waltham, MA) was used with 6uL of Lipofectamine 2000 (Invitrogen/Life Technologies, Carlsbad, CA).
668 Experimental condition wells were transfected with 1ug of the indicated construct of interest, 1ug of
669 HA-DHHC9 (mouse; Shimell et al., 2019), and 1ug of FLAG-GOLGA7 (Maurine Linder, Washington
670 University School of Medicine). Human FLAG-MOBP (CAT#: RC223946), FLAG-PLP1 (CAT#: RC218616)
671 and FLAG-CNP (CAT#: RC207038) were acquired from Origene, Maryland, USA. Control condition wells
672 were transfected with 1ug of the indicated construct of interest, and 2ug of a scrambled control
673 plasmid. Cells were lysed using the acyl-RAC assay lysis buffer 48hours after transfection.

674 **Palmitoylation Assay (acyl-RAC)**

675 The commercially available CAPTUREome S-palmitoylated protein kit (Badrilla, Leeds, UK) was used in
676 accordance with the manufacturer's guidelines with three optimizations: (1) prior to the cell lysis step,
677 wells were washed with 1mL of 1X PBS to eliminate any dead cells or residual media; (2) during the cell
678 lysis step, DNase (Sigma-Aldrich, St. Louis, MO), was added to the solution (5uL per 500uL of lysis
679 buffer); and (2) protein concentration was measured prior to the separation of experimental sample and
680 negative control sample using the BCA Assay (Pierce, Thermo Fisher Scientific, Waltham, MA).

681 **Western Blot Analysis**

682 Western blotting was performed using 4% stacking and 12% resolving SDS-PAGE gels. PVDF membranes
683 were then blocked for 1hour at room temperature with 5% BSA in 0.05% TBS-T. PVDF membranes were
684 incubated with the indicated primary antibodies (anti-HA: Cell Signaling Technology, C29F4, Rabbit mAb
685 CAT#: 3724, 1:1000; anti-FLAG: Origene, mouse monoclonal antibody, CAT#: TA50011-100, 1:1000)
686 overnight at 4°C. Proteins were then visualized using enhanced chemiluminescence (Immubilon Western
687 Chemiluminescent HRP Substrate) on a BioRad ChemiDoc XRS+ scanner. Blots were then quantified
688 using Fiji1 software. The palmitoylated and unpalmitoylated fractions were calculated using the
689 following equations respectively: (Palm Fraction / (Palm Fraction + Unpalm Fraction)) and (Unpalm
690 Fraction / (Palm Fraction + Unpalm Fraction)). Statistical analyses were performed in GraphPad Prism
691 9.2.0.

692 ## Acknowledgements

693 The authors would like to thank Drs. A Ciernia, M Cembrowski, T Murphy and J LeDue for helpful
694 discussion.

695 **References**

696 Abrami L, Dallavilla T, Sandoz PA, Demir M, Kunz B, Savoglidis G, Hatzimanikatis V, van Der Goot FG.
697 2017. Identification and dynamics of the human ZDHHC16-ZDHHC6 palmitoylation cascade. *eLife* **6**.
698 doi:10.7554/eLife.27826

699 Baker K, Astle DE, Scerif G, Barnes J, Smith J, Moffat G, Gillard J, Baldeweg T, Raymond FL. 2015.
700 Epilepsy, cognitive deficits and neuroanatomy in males with ZDHHC9 mutations. *Annals of Clinical*
701 *and Translational Neurology* **2**:559–569. doi:10.1002/acn3.196

702 Bathelt J, Astle D, Barnes J, Raymond FL, Baker K. 2016. Structural brain abnormalities in a single gene
703 disorder associated with epilepsy, language impairment and intellectual disability. *NeuroImage:*
704 *Clinical* **12**:655–665. doi:10.1016/j.nicl.2016.07.016

705 Bathelt J, Barnes J, Raymond FL, Baker K, Astle D. 2017. Global and Local Connectivity Differences
706 Converge With Gene Expression in a Neurodevelopmental Disorder of Known Genetic Origin.
707 *Cerebral Cortex* **27**:3806–3817. doi:10.1093/cercor/bhx027

708 Bird CM, Burgess N. 2008. The hippocampus and memory: Insights from spatial processing. *Nature*
709 *Reviews Neuroscience* **9**:182–194. doi:10.1038/nrn2335

710 Blanc M, David F, Abrami L, Migliozzi D, Armand F, Bürgi J, van der Goot FG. 2015. SwissPalm: Protein
711 Palmitoylation database. *F1000Research* **4**. doi:10.12688/f1000research.6464.1

712 Blanc M, David FPA, van der Goot FG. 2019. SwissPalm 2: Protein S-palmitoylation databaseMethods in
713 Molecular Biology. Humana Press Inc. pp. 203–214. doi:10.1007/978-1-4939-9532-5_16

714 Chen EY, Tan CM, Kou Y, Duan Q, Wang Z, Meirelles G V., Clark NR, Ma'ayan A. 2013. Enrichr: Interactive
715 and collaborative HTML5 gene list enrichment analysis tool. *BMC Bioinformatics* **14**.
716 doi:10.1186/1471-2105-14-128

717 Chen WY, Shi YY, Zheng YL, Zhao XZ, Zhang GJ, Chen SQ, Yang P Di, He L. 2004. Case-control study and
718 transmission disequilibrium test provide consistent evidence for association between
719 schizophrenia and genetic variation in the 22q11 gene ZDHHC8. *Human Molecular Genetics*
720 **13**:2991–2995. doi:10.1093/hmg/ddh322

721 Cho E, Park M. 2016. Palmitoylation in Alzheimer's disease and other neurodegenerative diseases.
722 *Pharmacological Research* **111**:133–151. doi:10.1016/j.phrs.2016.06.008

723 Forrester MT, Hess DT, Thompson JW, Hultman R, Moseley MA, Stamler JS, Casey PJ. 2011. Site-specific
724 analysis of protein S-acylation by resin-assisted capture. *Journal of Lipid Research* **52**:393–398.
725 doi:10.1194/JLR.D011106/ATTACHMENT/AA2B322B-A63D-41C0-A864-92DAC7C09076/MMC1.PDF

726 Fredericks G, Hoffmann F, Hondal R, Rozovsky S, Urschitz J, Hoffmann P. 2017. Selenoprotein K Increases
727 Efficiency of DHHC6 Catalyzed Protein Palmitoylation by Stabilizing the Acyl-DHHC6 Intermediate.
728 *Antioxidants* **7**:4. doi:10.3390/antiox7010004

729 Fredericks GJ, Hoffmann FKW, Rose AH, Osterheld HJ, Hess FM, Mercier F, Hoffmann PR. 2014. Stable
730 expression and function of the inositol 1,4,5-triphosphate receptor requires palmitoylation by a
731 DHHC6/selenoprotein K complex. *Proceedings of the National Academy of Sciences of the United*
732 *States of America* **111**:16478–16483. doi:10.1073/pnas.1417176111

733 Fukata Y, Dimitrov A, Boncompain G, Vielemeyer O, Perez F, Fukata M. 2013. Local palmitoylation cycles
734 define activity-regulated postsynaptic subdomains. *Journal of Cell Biology* **202**:145–161.
735 doi:10.1083/jcb.201302071

736 Fukata Y, Fukata M. 2010. Protein palmitoylation in neuronal development and synaptic plasticity.
737 *Nature Reviews Neuroscience* **11**:161–175. doi:10.1038/nrn2788

738 Glantz LA, Lewis DA. 2000. Decreased dendritic spine density on prefrontal cortical pyramidal neurons in
739 schizophrenia. *Archives of General Psychiatry* **57**:65–73. doi:10.1001/archpsyc.57.1.65

740 Globa AK, Bamji SX. 2017. Protein palmitoylation in the development and plasticity of neuronal
741 connections. *Current Opinion in Neurobiology* **45**:210–220. doi:10.1016/j.conb.2017.02.016

742 Gorinski N, Bijata M, Prasad S, Wirth A, Abdel Galil D, Zeug A, Bazovkina D, Kondaurova E, Kulikova E,
743 Ilchibaeva T, Zareba-Koziol M, Papaleo F, Scheggia D, Kochlamazashvili G, Dityatev A, Smyth I,
744 Krzystyniak A, Wlodarczyk J, Richter DW, Strekalova T, Sigrist S, Bang C, Hobuß L, Fiedler J, Thum T,
745 Naumenko VS, Pandey G, Ponimaskin E. 2019. Attenuated palmitoylation of serotonin receptor 5-
746 HT1A affects receptor function and contributes to depression-like behaviors. *Nature*
747 *Communications* **10**:1–14. doi:10.1038/s41467-019-11876-5

748 Haque A, Engel J, Teichmann SA, Lönnberg T. 2017. A practical guide to single-cell RNA-sequencing for
749 biomedical research and clinical applications. *Genome Medicine* **9**:1–12. doi:10.1186/s13073-017-
750 0467-4

751 Harris KD, Shepherd GMG. 2015. The neocortical circuit: Themes and variations. *Nature Neuroscience*
752 **18**:170–181. doi:10.1038/nn.3917

753 Ji B, Skup M. 2021. Roles of palmitoylation in structural long-term synaptic plasticity. *Molecular Brain*
754 **14**:1–27. doi:10.1186/s13041-020-00717-y

755 Kang R, Wan J, Arstikaitis P, Takahashi H, Huang K, Bailey AO, Thompson JX, Roth AF, Drisdel RC, Mastro
756 R, Green WN, Yates JR, Davis NG, El-Husseini A. 2008. Neural palmitoyl-proteomics reveals dynamic
757 synaptic palmitoylation. *Nature* **456**:904–909. doi:10.1038/nature07605

758 Karayiorgou M, Simon TJ, Gogos JA. 2010. 22q11.2 microdeletions: Linking DNA structural variation to
759 brain dysfunction and schizophrenia. *Nature Reviews Neuroscience* **11**:402–416.
760 doi:10.1038/nrn2841

761 Kolluri N, Sun Z, Sampson AR, Lewis DA. 2005. Lamina-specific reductions in dendritic spine density in
762 the prefrontal cortex of subjects with schizophrenia. *American Journal of Psychiatry* **162**:1200–
763 1202. doi:10.1176/appi.ajp.162.6.1200

764 Koopmans F, van Nierop P, Andres-Alonso M, Byrnes A, Cijsouw T, Coba MP, Cornelisse LN, Farrell RJ,
765 Goldschmidt HL, Howrigan DP, Hussain NK, Imig C, de Jong APH, Jung H, Kohansalnodehi M,
766 Kramarz B, Lipstein N, Lovering RC, MacGillavry H, Mariano V, Mi H, Ninov M, Osumi-Sutherland D,
767 Pielot R, Smalla KH, Tang H, Tashman K, Toonen RFG, Verpelli C, Reig-Viader R, Watanabe K, van
768 Weering J, Achsel T, Ashrafi G, Asi N, Brown TC, De Camilli P, Feuermann M, Foulger RE, Gaudet P,
769 Joglekar A, Kanellopoulos A, Malenka R, Nicoll RA, Pulido C, de Juan-Sanz J, Sheng M, Südhof TC,
770 Tilgner HU, Bagni C, Bayés À, Biederer T, Brose N, Chua JJE, Dieterich DC, Gundelfinger ED,
771 Hoogenraad C, Huganir RL, Jahn R, Kaeser PS, Kim E, Kreutz MR, McPherson PS, Neale BM,
772 O'Connor V, Posthuma D, Ryan TA, Sala C, Feng G, Hyman SE, Thomas PD, Smit AB, Verhage M.
773 2019. SynGO: An Evidence-Based, Expert-Curated Knowledge Base for the Synapse. *Neuron*
774 **103**:217-234.e4. doi:10.1016/j.neuron.2019.05.002

775 Koster KP, Yoshii A. 2019. Depalmitoylation by palmitoyl-protein thioesterase 1 in neuronal health and
776 degeneration. *Frontiers in Synaptic Neuroscience* **11**:25. doi:10.3389/fnsyn.2019.00025

777 Kouskou M, Thomson DM, Brett RR, Wheeler L, Tate RJ, Pratt JA, Chamberlain LH. 2018. Disruption of
778 the Zdhhc9 intellectual disability gene leads to behavioural abnormalities in a mouse model.
779 *Experimental Neurology* **308**:35–46. doi:10.1016/J.EXPNEUROL.2018.06.014

780 Kuleshov M V., Jones MR, Rouillard AD, Fernandez NF, Duan Q, Wang Z, Koplev S, Jenkins SL, Jagodnik
781 KM, Lachmann A, McDermott MG, Monteiro CD, Gundersen GW, Ma'ayan A. 2016. Enrichr: a
782 comprehensive gene set enrichment analysis web server 2016 update. *Nucleic acids research*
783 **44**:W90–W97. doi:10.1093/nar/gkw377

784 Lemonidis K, Sanchez-Perez MC, Chamberlain LH. 2015. Identification of a novel sequence motif
785 recognized by the ankyrin repeat domain of zDHHC17/13 S-acyltransferases. *Journal of Biological*
786 *Chemistry* **290**:21939–21950. doi:10.1074/jbc.M115.657668

787 Lin DTS, Conibear E. 2015. ABHD17 proteins are novel protein depalmitoylases that regulate N-Ras
788 palmitate turnover and subcellular localization. *eLife* **4**. doi:10.7554/eLife.11306

789 Lu JY, Verkruyse LA, Hofmann SL. 1996. Lipid thioesters derived from acylated proteins accumulate in
790 infantile neuronal ceroid lipofuscinosis: Correction of the defect in lymphoblasts by recombinant
791 palmitoyl-protein thioesterase. *Proceedings of the National Academy of Sciences of the United*
792 *States of America* **93**:10046–10050. doi:10.1073/pnas.93.19.10046

793 Ma Y, Liu H, Ou Z, Qi C, Xing R, Wang S, Han Y, Zhao T-J, Chen Y. 2021. DHHC5 facilitates oligodendrocyte
794 development by palmitoylating and activating STAT3. *Glia*. doi:10.1002/glia.24113

795 Malgapo MIP, Linder ME. 2021. Substrate recruitment by zDHHC protein acyltransferases. *Open Biology*
796 **11**:rsob.210026. doi:10.1098/rsob.210026

797 Marques S, Zeisel A, Codeluppi S, Van Bruggen D, Falcão AM, Xiao L, Li H, Häring M, Hochgerner H,
798 Romanov RA, Gyllborg D, Muñoz-Manchado AB, La Manno G, Lönnerberg P, Floriddia EM, Rezayee
799 F, Ernfors P, Arenas E, Hjerling-Leffler J, Harkany T, Richardson WD, Linnarsson S, Castelo-Branco G.
800 2016. Oligodendrocyte heterogeneity in the mouse juvenile and adult central nervous system.
801 *Science* **352**:1326–1329. doi:10.1126/science.aaf6463

802 Matt L, Kim K, Chowdhury D, Hell JW. 2019. Role of palmitoylation of postsynaptic proteins in promoting
803 synaptic plasticity. *Frontiers in Molecular Neuroscience*. doi:10.3389/fnmol.2019.00008

804 Mi H, Dong Q, Muruganujan A, Gaudet P, Lewis S, Thomas PD. 2009. PANTHER version 7: Improved
805 phylogenetic trees, orthologs and collaboration with the Gene Ontology Consortium. *Nucleic Acids*
806 *Research* **38**. doi:10.1093/nar/gkp1019

807 Mitchell DA, Hamel LD, Reddy KD, Farh L, Rettew LM, Sanchez PR, Deschenes RJ. 2014. Mutations in the

808 X-linked intellectual disability gene, zDHHC9, alter autopalmitoylation activity by distinct
809 mechanisms. *Journal of Biological Chemistry* **289**:18582–18592. doi:10.1074/jbc.M114.567420

810 Mukai J, Liu H, Burt RA, Swor DE, Lai WS, Karayiorgou M, Gogos JA. 2004. Evidence that the gene
811 encoding ZDHHC8 contributes to the risk of schizophrenia. *Nature Genetics* **36**:725–731.
812 doi:10.1038/ng1375

813 Nita DA, Mole SE, Minassian BA. 2016. Neuronal ceroid lipofuscinoses. *Epileptic Disorders* **18**:S73–S88.
814 doi:10.1684/epd.2016.0844

815 Pitts MW, Hoffmann PR. 2018. Endoplasmic reticulum-resident selenoproteins as regulators of calcium
816 signaling and homeostasis. *Cell Calcium* **70**:76–86. doi:10.1016/j.ceca.2017.05.001

817 Plain F, Howie J, Kennedy J, Brown E, Shattock MJ, Fraser NJ, Fuller W. 2020. Control of protein
818 palmitoylation by regulating substrate recruitment to a zDHHC-protein acyltransferase.
819 *Communications Biology* **3**:1–10. doi:10.1038/s42003-020-01145-3

820 Rana MS, Lee CJ, Banerjee A. 2018. The molecular mechanism of DHHC protein acyltransferases.
821 *Biochemical Society Transactions* **47**:157–167. doi:10.1042/BST20180429

822 Raymond FL, Tarpey PS, Edkins S, Tofts C, O'Meara S, Teague J, Butler A, Stevens C, Barthorpe S, Buck G,
823 Cole J, Dicks E, Gray K, Halliday K, Hills K, Hinton J, Jones D, Menzies A, Perry J, Raine K, Shepherd R,
824 Small A, Varian J, Widaa S, Mallya U, Moon J, Luo Y, Shaw M, Boyle J, Kerr B, Turner G, Quarrell O,
825 Cole T, Easton DF, Wooster R, Bobrow M, Schwartz CE, Gecz J, Stratton MR, Futreal PA. 2007.
826 Mutations in ZDHHC9, Which Encodes a Palmitoyltransferase of NRAS and HRAS, Cause X-Linked
827 Mental Retardation Associated with a Marfanoid Habitus. *The American Journal of Human Genetics*
828 **80**:982–987. doi:10.1086/513609

829 Roberts MS, Macauley SL, Wong AM, Yilmas D, Hohm S, Cooper JD, Sands MS. 2012. Combination small
830 molecule PPT1 mimetic and CNS-directed gene therapy as a treatment for infantile neuronal ceroid
831 lipofuscinosis. *Journal of Inherited Metabolic Disease* **35**:847–857. doi:10.1007/s10545-011-9446-x

832 Rocks O, Gerauer M, Vartak N, Koch S, Huang ZP, Pechlivanis M, Kuhlmann J, Brunsveld L, Chandra A,
833 Ellinger B, Waldmann H, Bastiaens PIH. 2010. The palmitoylation machinery is a spatially organizing
834 system for peripheral membrane proteins. *Cell* **141**:458–471. doi:10.1016/j.cell.2010.04.007

835 Rodenburg RNP, Snijder J, Van De Waterbeemd M, Schouten A, Granneman J, Heck AJR, Gros P. 2017.

836 Stochastic palmitoylation of accessible cysteines in membrane proteins revealed by native mass
837 spectrometry. *Nature Communications* **8**:1–9. doi:10.1038/s41467-017-01461-z

838 Rosenberg AB, Roco CM, Muscat RA, Kuchina A, Sample P, Yao Z, Graybuck LT, Peeler DJ, Mukherjee S,
839 Chen W, Pun SH, Sellers DL, Tasic B, Seelig G. 2018. Single-cell profiling of the developing mouse
840 brain and spinal cord with split-pool barcoding. *Science* **360**:176–182.
841 doi:10.1126/science.aam8999

842 Salaun C, Locatelli C, Zmuda F, González JC, Chamberlain LH. 2020. Accessory proteins of the zDHHC
843 family of S-acylation enzymes. *Journal of Cell Science* **133**. doi:10.1242/jcs.251819

844 Sanders SS, Martin DDO, Butland SL, Lavallée-Adam M, Calzolari D, Kay C, Yates JR, Hayden MR. 2015.
845 Curation of the Mammalian Palmitoylome Indicates a Pivotal Role for Palmitoylation in Diseases
846 and Disorders of the Nervous System and Cancers. *PLoS Computational Biology* **11**:e1004405.
847 doi:10.1371/journal.pcbi.1004405

848 Saunders A, Macosko EZ, Wysoker A, Goldman M, Krienen FM, de Rivera H, Bien E, Baum M, Bortolin L,
849 Wang S, Goeva A, Nemesh J, Kamitaki N, Brumbaugh S, Kulp D, McCarroll SA. 2018. Molecular
850 Diversity and Specializations among the Cells of the Adult Mouse Brain. *Cell* **174**:1015-1030.e16.
851 doi:10.1016/j.cell.2018.07.028

852 Schneider A, Länder H, Schulz G, Wolburg H, Nave K-A, Schulz JB, Simons M. 2005. Palmitoylation is a
853 sorting determinant for transport to the myelin membrane. *Journal of cell science* **118**:2415–23.
854 doi:10.1242/jcs.02365

855 Schwarz F, Aebi M. 2011. Mechanisms and principles of N-linked protein glycosylation. *Current Opinion*
856 *in Structural Biology* **21**:576–582. doi:10.1016/j.sbi.2011.08.005

857 Shimell JJ, Shah BS, Cain SM, Thouta S, Kuhlmann N, Tatarnikov I, Jovellar DB, Brigidi GS, Kass J,
858 Milnerwood AJ, Snutch TP, Bamji SX. 2019. The X-Linked Intellectual Disability Gene Zdhhc9 Is
859 Essential for Dendrite Outgrowth and Inhibitory Synapse Formation. *Cell Reports* **29**:2422-2437.e8.
860 doi:10.1016/j.celrep.2019.10.065

861 Shyng C, Nelvagal HR, Dearborn JT, Tyynelä J, Schmidt RE, Sands MS, Cooper JD. 2017. Synergistic effects
862 of treating the spinal cord and brain in CLN1 disease. *Proceedings of the National Academy of*
863 *Sciences of the United States of America* **114**:E5920–E5929. doi:10.1073/pnas.1701832114

Sjöstedt E, Zhong W, Fagerberg L, Karlsson M, Mitsios N, Adori C, Oksvold P, Edfors F, Limiszewska A, Hikmet F, Huang J, Du Y, Lin L, Dong Z, Yang L, Liu X, Jiang H, Xu X, Wang J, Yang H, Bolund L, Mardinoglu A, Zhang C, von Feilitzen K, Lindskog C, Pontén F, Luo Y, Hökfelt T, Uhlén M, Mulder J. 2020. An atlas of the protein-coding genes in the human, pig, and mouse brain. *Science* **367**:eaay5947. doi:10.1126/science.aay5947

Solis GP, Valnohova J, Alvarez C, Katanaev VL. 2020. Local and substrate-specific S-palmitoylation determines subcellular localization of Gαo. *bioRxiv* 2020.08.25.266692. doi:10.1101/2020.08.25.266692

Swarthout JT, Lobo S, Farh L, Croke MR, Greentree WK, Deschenes RJ, Linder ME. 2005. DHHC9 and GCP16 constitute a human protein fatty acyltransferase with specificity for H- and N-Ras. *Journal of Biological Chemistry* **280**:31141–31148. doi:10.1074/jbc.M504113200

Szklarczyk D, Gable AL, Lyon D, Junge A, Wyder S, Huerta-Cepas J, Simonovic M, Doncheva NT, Morris JH, Bork P, Jensen LJ, Von Mering C. 2019. STRING v11: Protein-protein association networks with increased coverage, supporting functional discovery in genome-wide experimental datasets. *Nucleic Acids Research* **47**:D607–D613. doi:10.1093/nar/gky1131

Tasic B, Yao Z, Graybuck LT, Smith KA, Nguyen TN, Bertagnolli D, Goldy J, Garren E, Economo MN, Viswanathan S, Penn O, Bakken T, Menon V, Miller J, Fong O, Hirokawa KE, Lathia K, Rimorin C, Tieu M, Larsen R, Casper T, Barkan E, Kroll M, Parry S, Shapovalova N V., Hirschstein D, Pendergraft J, Sullivan HA, Kim TK, Szafer A, Dee N, Groblewski P, Wickersham I, Cetin A, Harris JA, Levi BP, Sunkin SM, Madisen L, Daigle TL, Looger L, Bernard A, Phillips J, Lein E, Hawrylycz M, Svoboda K, Jones AR, Koch C, Zeng H. 2018. Shared and distinct transcriptomic cell types across neocortical areas. *Nature* **563**:72–78. doi:10.1038/s41586-018-0654-5

Thomas GM, Hayashi T, Chiu SL, Chen CM, Huganir RL. 2012. Palmitoylation by DHHC5/8 Targets GRIP1 to Dendritic Endosomes to Regulate AMPA-R Trafficking. *Neuron* **73**:482–496. doi:10.1016/j.neuron.2011.11.021

Thomas GM, Hayashi T, Huganir RL, Linden DJ. 2013. DHHC8-dependent PICK1 palmitoylation is required for induction of cerebellar long-term synaptic depression. *Journal of Neuroscience* **33**:15401–15407. doi:10.1523/JNEUROSCI.1283-13.2013

Tzschach A, Grasshoff U, Beck-Woedl S, Dufke C, Bauer C, Kehrer M, Evers C, Moog U, Oehl-Jaschkowitz

B, Donato N Di, Maiwald R, Jung C, Kuechler A, Schulz S, Meinecke P, Spranger S, Kohlhase J, Seidel J, Reif S, Rieger M, Riess A, Sturm M, Bickmann J, Schroeder C, Dufke A, Riess O, Bauer P. 2015. Next-generation sequencing in X-linked intellectual disability. *European Journal of Human Genetics* **23**:1513–1518. doi:10.1038/ejhg.2015.5

Ubersax JA, Ferrell JE. 2007. Mechanisms of specificity in protein phosphorylation. *Nature Reviews Molecular Cell Biology* **8**:530–541. doi:10.1038/nrm2203

Vartak N, Papke B, Grecco HE, Rossmannek L, Waldmann H, Hedberg C, Bastiaens PIH. 2014. The autodepalmitoylating activity of APT maintains the spatial organization of palmitoylated membrane proteins. *Biophysical Journal* **106**:93–105. doi:10.1016/j.bpj.2013.11.024

Verardi R, Kim JS, Ghirlando R, Banerjee A. 2017. Structural Basis for Substrate Recognition by the Ankyrin Repeat Domain of Human DHHC17 Palmitoyltransferase. *Structure* **25**:1337-1347.e6. doi:10.1016/j.str.2017.06.018

Virlogeux A, Scaramuzzino C, Lenoir S, Carpentier R, Louessard M, Genoux A, Lino P, Hinckelmann MV, Perrier AL, Humbert S, Saudou F. 2021. Increasing brain palmitoylation rescues behavior and neuropathology in Huntington disease mice. *Science Advances* **7**:799–830. doi:10.1126/sciadv.abb0799

Wagstyl K, Ronan L, Whitaker KJ, Goodyer IM, Roberts N, Crow TJ, Fletcher PC. 2016. Multiple markers of cortical morphology reveal evidence of supragranular thinning in schizophrenia. *Translational Psychiatry* **6**:780. doi:10.1038/tp.2016.43

Woodley KT, Collins MO. 2019. S-acylated Golga7b stabilises <scp>DHHC</scp> 5 at the plasma membrane to regulate cell adhesion. *EMBO reports* **20**:e47472. doi:10.15252/embr.201847472

Yanai A, Huang K, Kang R, Singaraja RR, Arstikaitis P, Gan L, Orban PC, Mullard A, Cowan CM, Raymond LA, Drisdel RC, Green WN, Ravikumar B, Rubinsztein DC, El-Husseini A, Hayden MR. 2006. Palmitoylation of huntingtin by HIP14is essential for its trafficking and function. *Nature Neuroscience* **9**:824–831. doi:10.1038/nn1702

Yao Z, van Velthoven CTJ, Nguyen TN, Goldy J, Sedeno-Cortes AE, Baftizadeh F, Bertagnolli D, Casper T, Chiang M, Crichton K, Ding SL, Fong O, Garren E, Glandon A, Gouwens NW, Gray J, Graybuck LT, Hawrylycz MJ, Hirschstein D, Kroll M, Lathia K, Lee C, Levi B, McMillen D, Mok S, Pham T, Ren Q, Rimorin C, Shapovalova N, Sulc J, Sunkin SM, Tieu M, Torkelson A, Tung H, Ward K, Dee N, Smith

922 KA, Tasic B, Zeng H. 2021. A taxonomy of transcriptomic cell types across the isocortex and
923 hippocampal formation. *Cell* **184**:3222-3241.e26. doi:10.1016/j.cell.2021.04.021

924 Yuan W, Lu L, Rao M, Huang Y, Liu CE, Liu S, Zhao Y, Liu H, Zhu J, Chao T, Wu C, Ren J, Lv L, Li W, Qi S,
925 Liang Y, Yue S, Gao J, Zhang Z, Kong E. 2021. GFAP hyperpalmitoylation exacerbates astrogliosis and
926 neurodegenerative pathology in PPT1-deficient mice. *Proceedings of the National Academy of*
927 *Sciences of the United States of America* **118**. doi:10.1073/pnas.2022261118

928 Zareba-Koziol M, Bartkowiak-Kaczmarek A, Figiel I, Krzystyniak A, Wojtowicz T, Bijata M, Wlodarczyk J.
929 2019. Stress-induced Changes in the S-palmitoylation and S-nitrosylation of Synaptic Proteins.
930 *Molecular and Cellular Proteomics* **18**:1916–1938. doi:10.1074/mcp.RA119.001581

931 Zeisel A, Hochgerner H, Lönnerberg P, Johnsson A, Memic F, van der Zwan J, Häring M, Braun E, Borm LE,
932 La Manno G, Codeluppi S, Furlan A, Lee K, Skene N, Harris KD, Hjerling-Leffler J, Arenas E, Ernfors P,
933 Marklund U, Linnarsson S. 2018. Molecular Architecture of the Mouse Nervous System. *Cell*
934 **174**:999-1014.e22. doi:10.1016/j.cell.2018.06.021

935 Zeisel A, M͡oz-Manchado AB, Codeluppi S, Lönnerberg P, Manno G La, Juréus A, Marques S, Munguba H,
936 He L, Betsholtz C, Rolny C, Castelo-Branco G, Hjerling-Leffler J, Linnarsson S. 2015. Cell types in the
937 mouse cortex and hippocampus revealed by single-cell RNA-seq. *Science* **347**:1138–1142.
938 doi:10.1126/science.aaa1934

939

Figure1

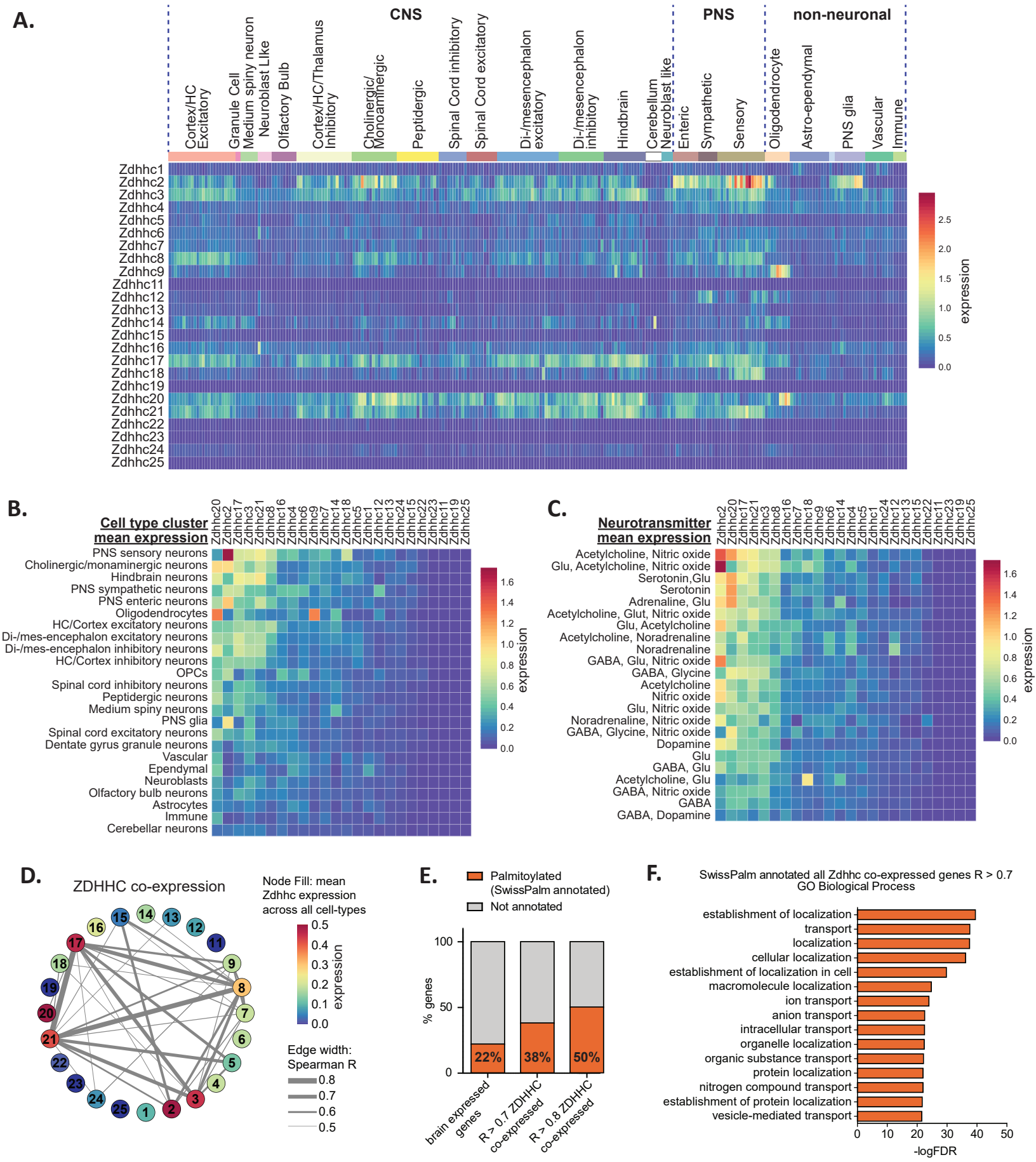
A.
CNS
PNS
non-neuronal
Cortex/HC Excitatory
Granule Cell
Medium spiny neuron
Neuroblast LIke
Olfactory Bulb
Cortex/HC/Thalamus Inhibitory
Cholinergic/ Monoaminergic
Peptidergic
Spinal Cord inhibitory
Spinal Cord excitatory
Di-/mesencephalon excitatory
Di-/mesencephalon inhibitory
Hindbrain
Cerebellum
Neuroblast like
Enteric
Sympathetic
Sensory
Oligodendrocyte
Astro-ependymal
PNS glia
Vascular
Immune
Zdhhc1
Zdhhc2
Zdhhc3
Zdhhc4
Zdhhc5
Zdhhc6
Zdhhc7
Zdhhc8
Zdhhc9
Zdhhc11
Zdhhc12
Zdhhc13
Zdhhc14
Zdhhc15
Zdhhc16
Zdhhc17
Zdhhc18
Zdhhc19
Zdhhc20
Zdhhc21
Zdhhc22
Zdhhc23
Zdhhc24
Zdhhc25
expression
B.
Cell type cluster mean expression
PNS sensory neurons
Cholinergic/monaminergic neurons
Hindbrain neurons
PNS sympathetic neurons
PNS enteric neurons
Oligodendrocytes
HC/Cortex excitatory neurons
Di-/mes-encephalon excitatory neurons
Di-/mes-encephalon inhibitory neurons
HC/Cortex inhibitory neurons
OPCs
Spinal cord inhibitory neurons
Peptidergic neurons
Medium spiny neurons
PNS glia
Spinal cord excitatory neurons
Dentate gyrus granule neurons
Vascular
Ependymal
Neuroblasts
Olfactory bulb neurons
Astrocytes
Immune
Cerebellar neurons
C.
Neurotransmitter mean expression
Acetylcholine, Nitric oxide
Glu, Acetylcholine, Nitric oxide
Serotonin,Glu
Serotonin
Adrenaline, Glu
Acetylcholine, Glut, Nitric oxide
Glu, Acetylcholine
Acetylcholine, Noradrenaline
Noradrenaline
GABA, Glu, Nitric oxide
GABA, Glycine
Acetylcholine
Nitric oxide
Glu, Nitric oxide
Noradrenaline, Nitric oxide
GABA, Glycine, Nitric oxide
Dopamine
Glu
GABA, Glu
Acetylcholine, Glu
GABA, Nitric oxide
GABA
GABA, Dopamine
D.
ZDHHC co-expression
Node Fill: mean Zdhhc expression across all cell-types
Edge width: Spearman R
E.
Palmitoylated (SwissPalm annotated)
Not annotated
% genes
22%
38%
50%
brain expressed genes
R > 0.7 ZDHHC co-expressed
R > 0.8 ZDHHC co-expressed
F.
SwissPalm annotated all Zdhhc co-expressed genes R > 0.7
GO Biological Process
establishment of localization
transport
localization
cellular localization
establishment of localization in cell
macromolecule localization
ion transport
anion transport
intracellular transport
organelle localization
organic substance transport
protein localization
nitrogen compound transport
establishment of protein localization
vesicle-mediated transport
-logFDR

Figure 2

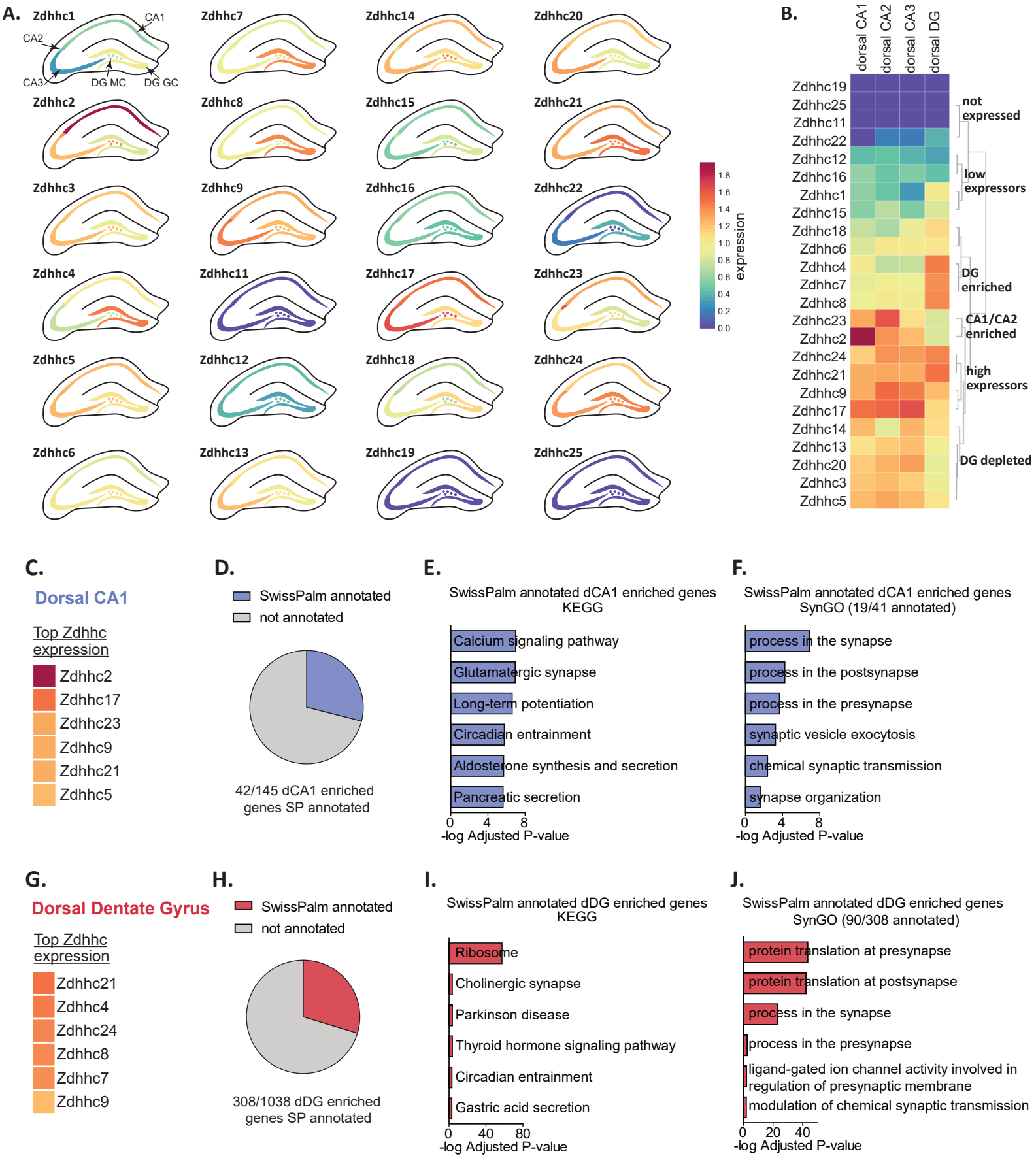
A.
Zdhhc1
CA1
CA2
CA3
DG MC
DG GC
Zdhhc2
Zdhhc3
Zdhhc4
Zdhhc5
Zdhhc6
Zdhhc7
Zdhhc8
Zdhhc9
Zdhhc11
Zdhhc12
Zdhhc13
Zdhhc14
Zdhhc15
Zdhhc16
Zdhhc17
Zdhhc18
Zdhhc19
Zdhhc20
Zdhhc21
Zdhhc22
Zdhhc23
Zdhhc24
Zdhhc25
expression
1.8
1.6
1.4
1.2
1.0
0.8
0.6
0.4
0.2
0.0
B.
dorsal CA1
dorsal CA2
dorsal CA3
dorsal DG
Zdhhc19
Zdhhc25
Zdhhc11
Zdhhc22
Zdhhc12
Zdhhc16
Zdhhc1
Zdhhc15
Zdhhc18
Zdhhc6
Zdhhc4
Zdhhc7
Zdhhc8
Zdhhc23
Zdhhc2
Zdhhc24
Zdhhc21
Zdhhc9
Zdhhc17
Zdhhc14
Zdhhc13
Zdhhc20
Zdhhc3
Zdhhc5
not expressed
low expressors
DG enriched
CA1/CA2 enriched
high expressors
DG depleted
C.
Dorsal CA1
Top Zdhhc expression
Zdhhc2
Zdhhc17
Zdhhc23
Zdhhc9
Zdhhc21
Zdhhc5
D.
SwissPalm annotated
not annotated
42/145 dCA1 enriched genes SP annotated
E.
SwissPalm annotated dCA1 enriched genes KEGG
Calcium signaling pathway
Glutamatergic synapse
Long-term potentiation
Circadian entrainment
Aldosterone synthesis and secretion
Pancreatic secretion
0
4
8
-log Adjusted P-value
F.
SwissPalm annotated dCA1 enriched genes SynGO (19/41 annotated)
process in the synapse
process in the postsynapse
process in the presynapse
synaptic vesicle exocytosis
chemical synaptic transmission
synapse organization
0
4
8
-log Adjusted P-value
G.
Dorsal Dentate Gyrus
Top Zdhhc expression
Zdhhc21
Zdhhc4
Zdhhc24
Zdhhc8
Zdhhc7
Zdhhc9
H.
SwissPalm annotated
not annotated
308/1038 dDG enriched genes SP annotated
I.
SwissPalm annotated dDG enriched genes KEGG
Ribosome
Cholinergic synapse
Parkinson disease
Thyroid hormone signaling pathway
Circadian entrainment
Gastric acid secretion
0
40
80
-log Adjusted P-value
J.
SwissPalm annotated dDG enriched genes SynGO (90/308 annotated)
protein translation at presynapse
protein translation at postsynapse
process in the synapse
process in the presynapse
ligand-gated ion channel activity involved in regulation of presynaptic membrane
modulation of chemical synaptic transmission
0
20
40
-log Adjusted P-value

Figure 3

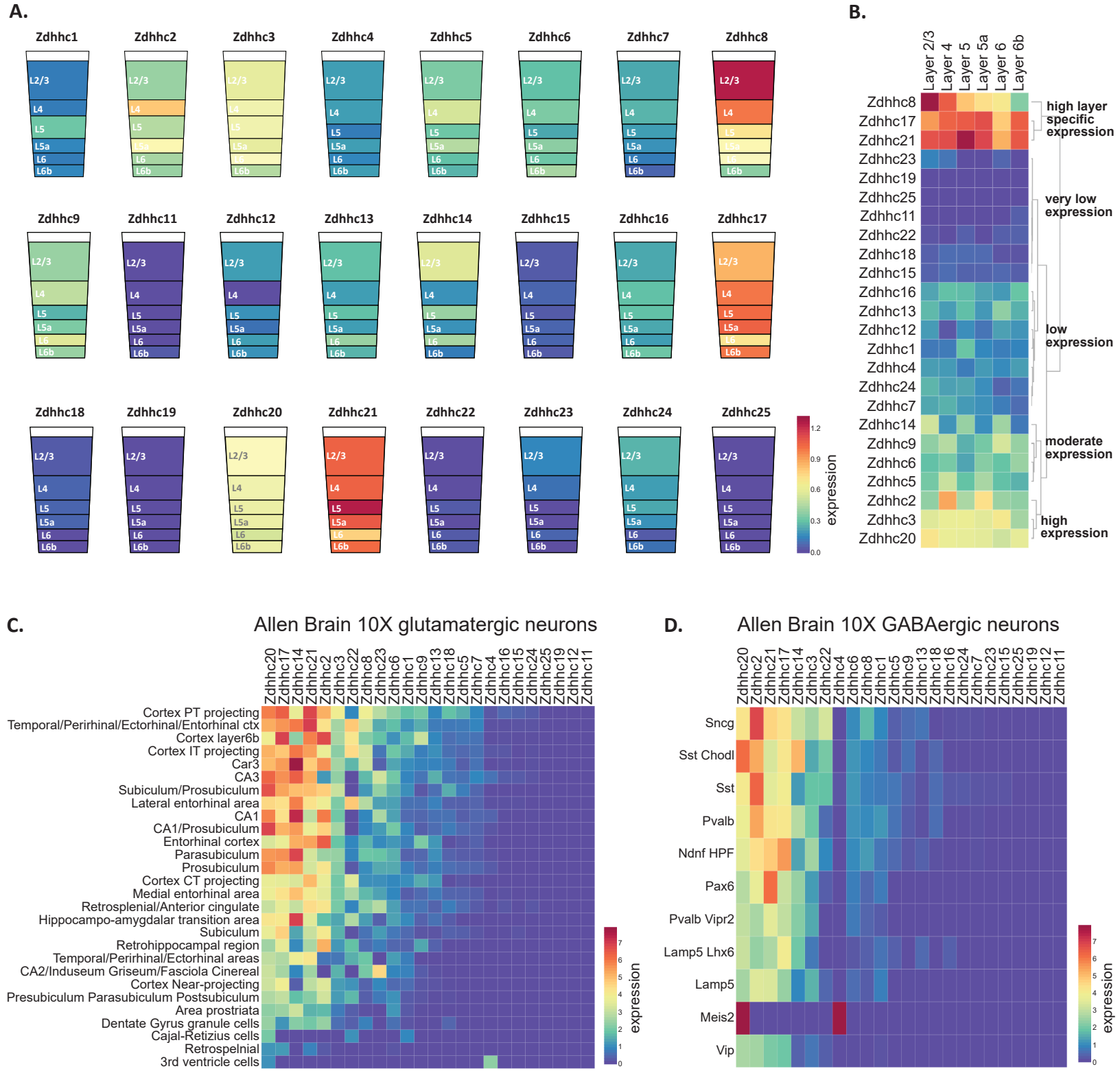
A.
Zdhhc1
Zdhhc2
Zdhhc3
Zdhhc4
Zdhhc5
Zdhhc6
Zdhhc7
Zdhhc8
Zdhhc9
Zdhhc11
Zdhhc12
Zdhhc13
Zdhhc14
Zdhhc15
Zdhhc16
Zdhhc17
Zdhhc18
Zdhhc19
Zdhhc20
Zdhhc21
Zdhhc22
Zdhhc23
Zdhhc24
Zdhhc25
L2/3
L4
L5
L5a
L6
L6b
expression
B.
Layer 2/3
Layer 4
Layer 5
Layer 5a
Layer 6
Layer 6b
high layer specific expression
very low expression
low expression
moderate expression
high expression
C.
Allen Brain 10X glutamatergic neurons
Cortex PT projecting
Temporal/Perirhinal/Ectorhinal/Entorhinal ctx
Cortex layer6b
Cortex IT projecting
Car3
CA3
Subiculum/Prosubiculum
Lateral entorhinal area
CA1
CA1/Prosubiculum
Entorhinal cortex
Parasubiculum
Prosubiculum
Cortex CT projecting
Medial entorhinal area
Retrosplenial/Anterior cingulate
Hippocampo-amygdalar transition area
Subiculum
Retrohippocampal region
Temporal/Perirhinal/Ectorhinal areas
CA2/Induseum Griseum/Fasciola Cinereal
Cortex Near-projecting
Presubiculum Parasubiculum Postsubiculum
Area prostriata
Dentate Gyrus granule cells
Cajal-Retizius cells
Retrospelnial
3rd ventricle cells
D.
Allen Brain 10X GABAergic neurons
Sncg
Sst Chodl
Sst
Pvalb
Ndnf HPF
Pax6
Pvalb Vipr2
Lamp5 Lhx6
Lamp5
Meis2
Vip

Figure 4

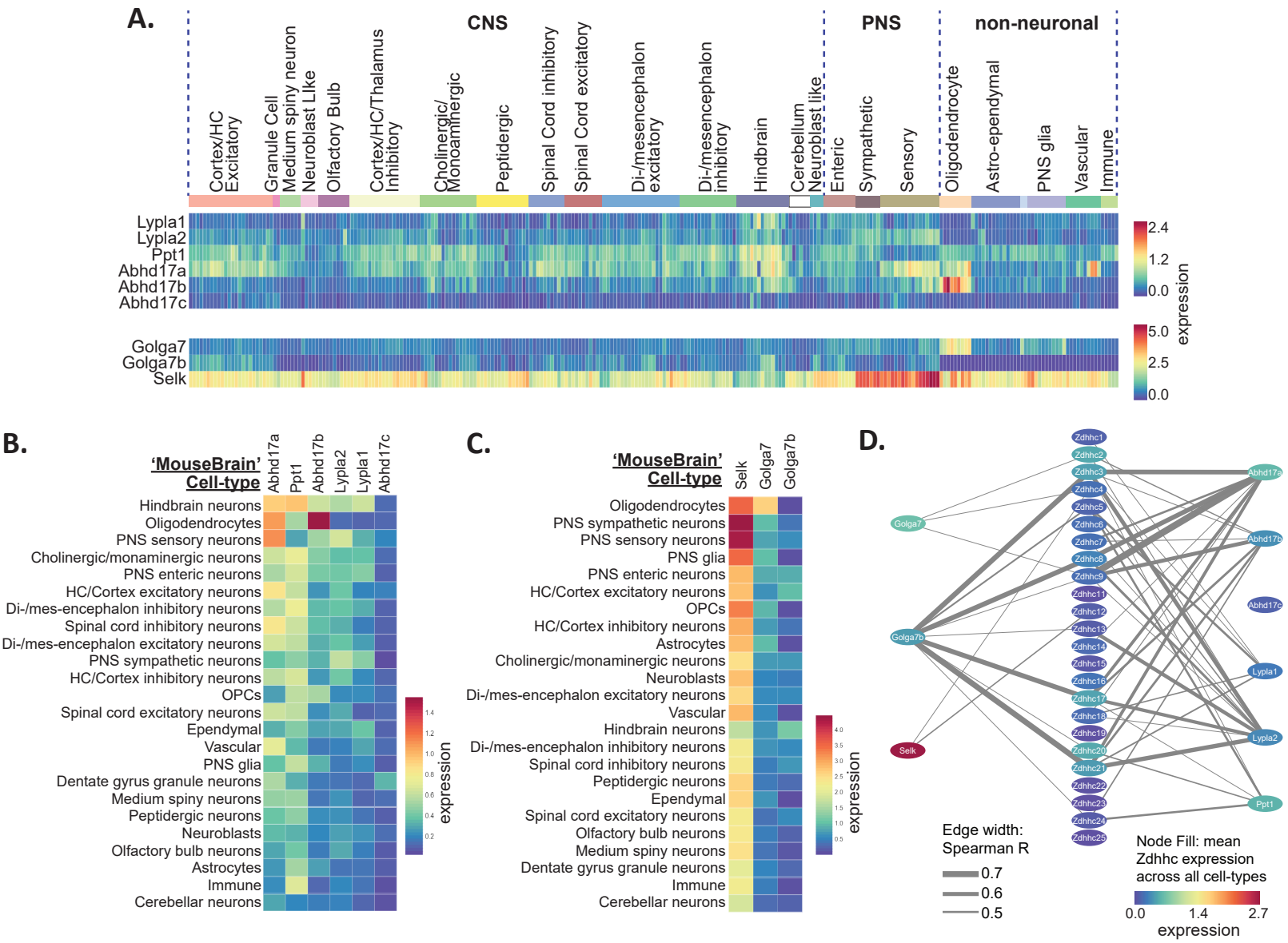
A.
CNS
PNS
non-neuronal
Cortex/HC Excitatory
Granule Cell
Medium spiny neuron
Neuroblast Like
Olfactory Bulb
Cortex/HC/Thalamus Inhibitory
Cholinergic/ Monoaminergic
Peptidergic
Spinal Cord inhibitory
Spinal Cord excitatory
Di-/mesencephalon excitatory
Di-/mesencephalon inhibitory
Hindbrain
Cerebellum
Neuroblast like
Enteric
Sympathetic
Sensory
Oligodendrocyte
Astro-ependymal
PNS glia
Vascular
Immune
Lypla1
Lypla2
Ppt1
Abhd17a
Abhd17b
Abhd17c
Golga7
Golga7b
Selk
2.4
1.2
0.0
expression
5.0
2.5
0.0
B.
'MouseBrain' Cell-type
Abhd17a
Ppt1
Abhd17b
Lypla2
Lypla1
Abhd17c
Hindbrain neurons
Oligodendrocytes
PNS sensory neurons
Cholinergic/monaminergic neurons
PNS enteric neurons
HC/Cortex excitatory neurons
Di-/mes-encephalon inhibitory neurons
Spinal cord inhibitory neurons
Di-/mes-encephalon excitatory neurons
PNS sympathetic neurons
HC/Cortex inhibitory neurons
OPCs
Spinal cord excitatory neurons
Ependymal
Vascular
PNS glia
Dentate gyrus granule neurons
Medium spiny neurons
Peptidergic neurons
Neuroblasts
Olfactory bulb neurons
Astrocytes
Immune
Cerebellar neurons
expression
C.
'MouseBrain' Cell-type
Selk
Golga7
Golga7b
Oligodendrocytes
PNS sympathetic neurons
PNS sensory neurons
PNS glia
PNS enteric neurons
HC/Cortex excitatory neurons
OPCs
HC/Cortex inhibitory neurons
Astrocytes
Cholinergic/monaminergic neurons
Neuroblasts
Di-/mes-encephalon excitatory neurons
Vascular
Hindbrain neurons
Di-/mes-encephalon inhibitory neurons
Spinal cord inhibitory neurons
Peptidergic neurons
Ependymal
Spinal cord excitatory neurons
Olfactory bulb neurons
Medium spiny neurons
Dentate gyrus granule neurons
Immune
Cerebellar neurons
expression
D.
Golga7
Golga7b
Selk
Zdhhc1
Zdhhc2
Zdhhc3
Zdhhc4
Zdhhc5
Zdhhc6
Zdhhc7
Zdhhc8
Zdhhc9
Zdhhc11
Zdhhc12
Zdhhc13
Zdhhc14
Zdhhc15
Zdhhc16
Zdhhc17
Zdhhc18
Zdhhc19
Zdhhc20
Zdhhc21
Zdhhc22
Zdhhc23
Zdhhc24
Zdhhc25
Abhd17a
Abhd17b
Abhd17c
Lypla1
Lypla2
Ppt1
Edge width: Spearman R
0.7
0.6
0.5
Node Fill: mean Zdhhc expression across all cell-types
0.0
1.4
2.7
expression

Figure 5

A. ***Zdhhc8*** **neonatal expression Rosenberg et al <P11**

- Cortex/HC neuron
- Midbrain/hindbrain neuron
- Olfactory neuron
- Migrating interneuron
- Oligodendrocyte
- Cerebellum neuron
- Microglia
- Spinal cord neuron
- OPC
- Vascular
- Astrocyte
- Ependymal
- Macrophage

0.14 0.07 0.0

B. ***Zdhhc8*** **adolescent expression 'MouseBrain' P25**

- Cortex/HC neuron
- Midbrain/hindbrain neuron
- Interneuron
- Spinal cord neuron
- Oligodendrocyte
- Vascular
- Cerebellum neuron
- Olfactory neuron
- OPC
- Astrocytes
- Ependymal
- Microglia
- Macrophage

0.5 0.25 0.0

C. ***Zdhhc8*** **adult expression 'Protein Atlas' Mouse P60**

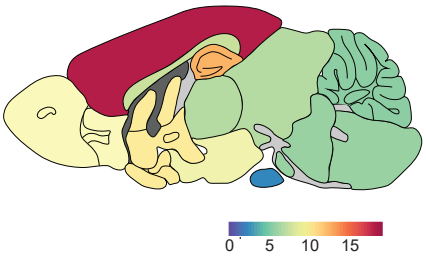

D. ***Zdhhc9*** **neonatal expression Rosenberg et al <P11**

- Oligodendrocyte
- Midbrain/hindbrain neuron
- Cortex/HC neuron
- Olfactory neuron
- Spinal cord neuron
- Macrophage
- Migrating interneuron
- Cerebellum neuron
- Vascular
- Microglia
- OPC
- Ependymal
- Astrocyte

0.28 0.14 0.0

E. ***Zdhhc9*** **adolescent expression 'MouseBrain' P25**

- Oligodendrocyte
- Cortex/HC neuron
- Midbrain/hindbrain neuron
- Vascular
- Interneuron
- Spinal cord neuron
- Ependymal
- OPC
- Cerebellum neuron
- Macrophage
- Olfactory neuron
- Astrocytes
- Microglia

1.0 0.5 0.0

F. ***Zdhhc9*** **adult expression 'Protein Atlas' Mouse P60**

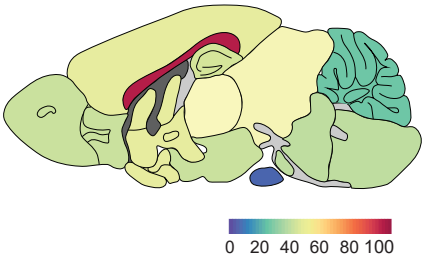

G. ***Ppt1*** **neonatal expression Rosenberg et al <P11**

- Olfactory neuron
- Spinal cord neuron
- Microglia
- Midbrain/hindbrain neuron
- Cortex/HC neuron
- Migrating interneuron
- Cerebellum neuron
- Astrocyte
- OPC
- Oligodendrocyte
- Ependymal
- Vascular
- Macrophage

1.5 0.75 0.0

H. ***Ppt1*** **adolescent expression 'MouseBrain' P25**

- Microglia
- Interneuron
- Midbrain/hindbrain neuron
- Macrophage
- Cortex/HC neuron
- Spinal cord neuron
- OPC
- Oligodendrocyte
- Astrocytes
- Ependymal
- Olfactory neuron
- Vascular
- Cerebellum neuron

0.6 0.3 0.0

I. ***Ppt1*** **adult expression 'Protein Atlas' Mouse P60**

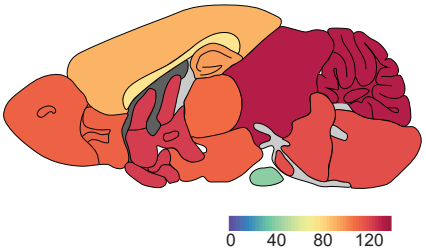

Figure 6

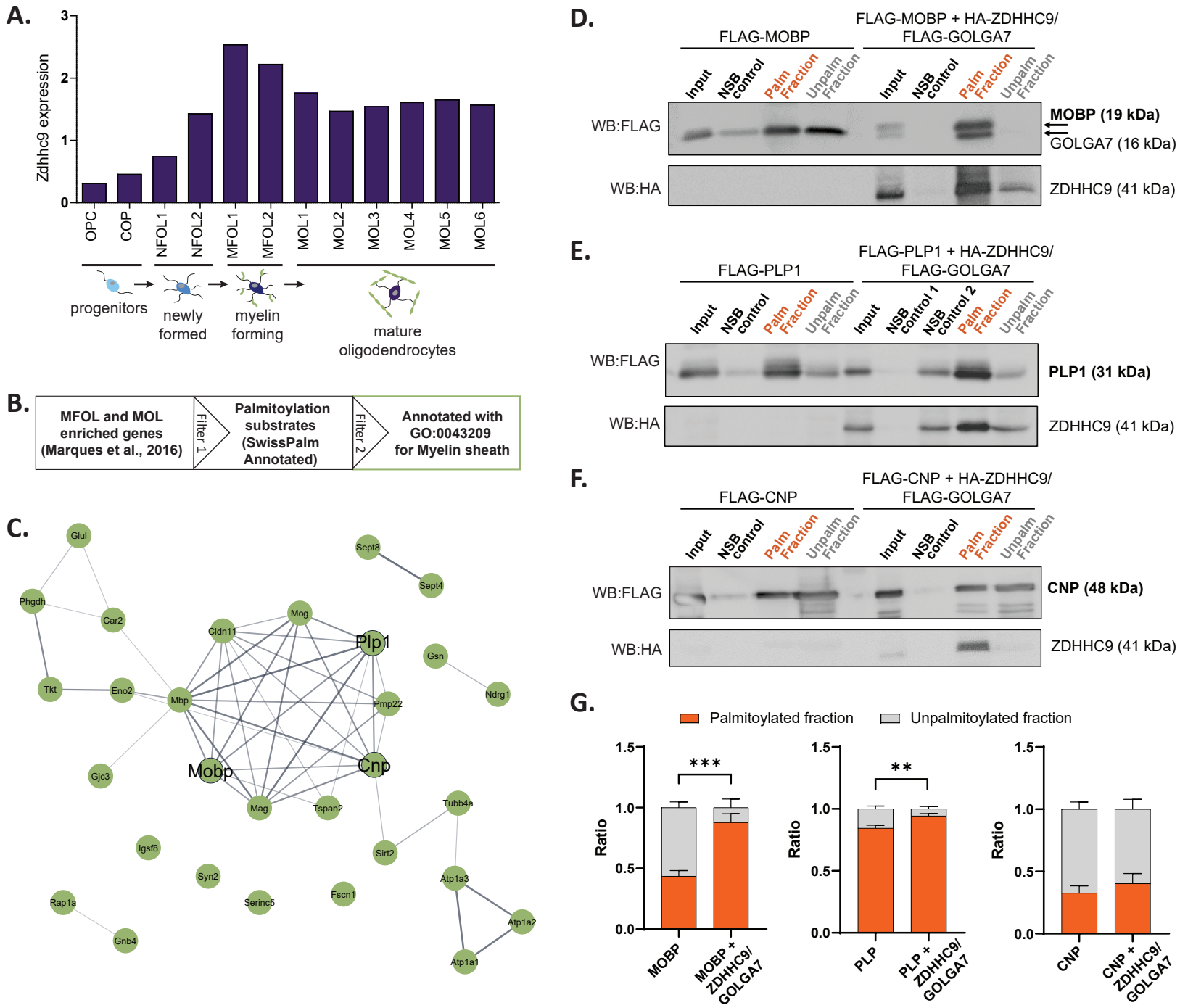
A.
Zdhhc9 expression
0
1
2
3
OPC
COP
NFOL1
NFOL2
MFOL1
MFOL2
MOL1
MOL2
MOL3
MOL4
MOL5
MOL6
progenitors
newly formed
myelin forming
mature oligodendrocytes
B.
MFOL and MOL enriched genes (Marques et al., 2016)
Filter 1
Palmitoylation substrates (SwissPalm Annotated)
Filter 2
Annotated with GO:0043209 for Myelin sheath
C.
Glul
Phgdh
Car2
Tkt
Eno2
Mbp
Gjc3
Mobp
Mag
Tspan2
Cldn11
Mog
Plp1
Pmp22
Cnp
Sept8
Sept4
Gsn
Ndrg1
Tubb4a
Sirt2
Atp1a3
Atp1a2
Atp1a1
Igsf8
Syn2
Rap1a
Gnb4
Serinc5
Fscn1
D.
FLAG-MOBP
FLAG-MOBP + HA-ZDHHC9/ FLAG-GOLGA7
Input
NSB control
Palm Fraction
Unpalm Fraction
WB:FLAG
WB:HA
MOBP (19 kDa)
GOLGA7 (16 kDa)
ZDHHC9 (41 kDa)
E.
FLAG-PLP1
FLAG-PLP1 + HA-ZDHHC9/ FLAG-GOLGA7
NSB control 1
NSB control 2
PLP1 (31 kDa)
F.
FLAG-CNP
FLAG-CNP + HA-ZDHHC9/ FLAG-GOLGA7
CNP (48 kDa)
G.
Palmitoylated fraction
Unpalmitoylated fraction
Ratio
***
**
MOBP
MOBP + ZDHHC9/ GOLGA7
PLP
PLP + ZDHHC9/ GOLGA7
CNP
CNP + ZDHHC9/ GOLGA7